ELSEVIER

Advanced characterization techniques for solid state lithium battery research

Yuxuan Xiang [1,†], Xia Li [2,†], Yongqiang Cheng [3,†], Xueliang Sun [2,*], Yong Yang [1,*]

[1] State Key Laboratory for Physical Chemistry of Solid Surfaces, Collaborative Innovation Center of Chemistry for Energy Materials and Department of Chemistry, College of Chemistry and Chemical Engineering, Xiamen University, Xiamen 361005, China
[2] Department of Mechanical and Materials Engineering, University of Western Ontario, London, Ontario N6A 5B9, Canada
[3] Neutron Scattering Division, Oak Ridge National Laboratory, Oak Ridge, TN, USA

Solid state batteries have attracted significant attention within the battery community over the last decade, due to the feasibility of developing a new generation of rechargeable Li batteries offering safer and long-term performance. However, many scientific and technical challenges and difficulties still need to be overcome before this new technology can be used commercially. Advanced characterization techniques provide powerful tools for studying these complex and elusive chemical/physical processes in solid-state batteries. Over the last decade, researchers have explored many sophisticated ex-situ and in-situ techniques, such as synchrotron X-ray techniques, solid-state NMR techniques, neutron scattering techniques, etc., to probe the undisclosed underlying mechanisms of solid-state batteries. In this review, we present a comprehensive overview of recent advances in these three characterization techniques in solid state battery research. Some perspectives of the future evolution of the techniques are also presented.

Introduction

Among the various energy storage devices, lithium-ion batteries, with their high energy density, scale flexibility, and low maintenance cost, have been successfully applied in our society. However, due to the intrinsic limitation of available battery materials, lithium-ion batteries will approach a bottleneck in the near future [1,2]. It is therefore imperative to develop a new generation of energy storage devices. As a candidate for next-generation energy storage devices, Lithium Metal Batteries (LMBs) are attracting more and more attention in academia and industry due to the high specific capacity (3860 mA h g^{-1}) and operating voltage [1]. However, the practical application of LMBs is hindered by the low coulombic efficiency and the growth of Li dendrite, which could pose a serious safety hazard if it is associated with flammable organic electrolytes [3]. The replacement of organic liquid electrolytes with solid-state electrolytes (SSEs) to assemble the solid-state batteries (SSBs), whose components are all in solid-state, which is expected to address these safety concerns fundamentally. In addition, SSBs also allow the application of high voltage and Li-free cathodes to achieve higher energy density [4].

Unfortunately, in the practical applications, SSBs always show less capacity, poor cycle performance and rapid capacity degradation due to the following scientific/technological concerns: (i) poor ionic conductivity of SSEs (10^{-6}–10^{-3} S cm^{-1}) relative to the liquid electrolyte (10^{-2} S cm^{-1}); (ii) the incompatibility between the electrode materials||SSE interface, including physical interface contact, parasitic reactions and formation of a space charge layer [4,5]. For example, the poor-wetting properties between lithium metal and $Li_7La_3Zr_2O_{12}$ (LLZO) will result in significant interfacial impedance [6,7]; (iii) uncontrollable growth of lithium dendrite even in the grain boundary within the solid electrolytes [3]. Towards a complete understanding of ionic diffusion in SSEs, as well as the complex and elusive interface reaction, is the cornerstone of improving the cycle performance of SSBs. In this regard, much progress has been made in developing

* Corresponding authors.
E-mail addresses: Sun, X. (xsun@eng.uwo.ca), Yang, Y. (yyang@xmu.edu.cn).
† Contributed equally to this review paper.

1369-7021/© 2020 Elsevier Ltd. All rights reserved. https://doi.org/10.1016/j.mattod.2020.01.018

advanced characterization techniques to probe SSBs from different perspectives to provide guidelines for SSBs optimization [8,9]. The limited light/electron permeability of SSBs poses insurmountable obstacles for studying their bulk structure and interface reactions with light and electrons. For example, the electron microscopy techniques, such as scanning transmission electron microscopy (STEM) and transmission electron microscopy (TEM), require careful sample processing and it is difficult to study the reaction at the solid–solid interface in-situ or in-operando. In this case, some spectroscopic methods show unique superiority in the research of SSBs due to their unique penetrability in opaque solids. For example, the versatile synchrotron X-ray techniques that include scattering, spectroscopy and imaging techniques, have been widely applied in investigating structural and chemical information of SSBs [10]. Similar to X-ray scattering, neutron scattering (ND) is another useful technique for probing the atomic structure and is more sensitive to light elements such as Li, O, Na, which is conducive to locating the position of light elements. ND also excels in measuring diffusion and vibrational dynamics. Compared to synchrotron X-ray techniques and ND that require the large-scale facility, laboratory-scale solid-state magnetic resonance (SS NMR) can be more conveniently used. Complemented with various NMR methods, such as magic angle spinning (MAS), pulse field gradient (PFG), and imaging techniques, a wealth of information about atomic occupancy, ionic motion, and morphology can be obtained [11].

In this article, we examine recent developments and progress in advanced characterization techniques in SSB research, including synchrotron X-ray techniques, solid-state NMR, and neutron scattering techniques. Each technique will be elaborated from the point of view of the intrinsic properties of SSEs and interfacial issues, respectively. Limited by the size and scope of this article, typical examples are chosen to illustrate what we can learn from these advanced characterization methods and we hope to initiate a reference to induce more valuable discussions.

Synchrotron X-ray techniques

Synchrotron radiation (SR) is a powerful tool for studying the fundamental working mechanism of battery materials [10]. The developed high flux and brilliance with a broad spectrum of the X-ray beams enables it to meet a variety of characterization demands, involving scattering, spectroscopy, and imaging techniques, to obtain structural and chemical information with different levels of spatial and temporal length scales [12]. The characteristics of SR techniques include [13,14] (i) high brilliance and finely tunable energies of the X-ray beam, which provides high structural resolution, such as crystalline structure, electronic structure, chemical composition, as well as 2D and 3D morphological information of battery materials. (ii) High temporal resolution, such as time-resolved XRD and XAS. For example, time-resolved XAS reduces the experimental time scale to milliseconds, capturing the dynamic nature of battery materials in a fast-transient process. (iii) Multiple spatial resolutions from nano- to microscale X-ray images, providing opportunities for direct visualization and 3D reconstruction of battery materials, and, therefore, providing information on the microstructure, morphology, and chemical distribution of materials. (iv) In-situ/operando X-ray techniques, which continuously monitor electrochemical, physical and chemical processes during electrochemical and chemical reactions. In recent decades, synchrotron X-ray techniques have demonstrated their great importance in characterizing the physical and chemical properties of battery materials in order to reveal fundamental mechanisms and guide the technological optimization of batteries [14–17]. Readers who interest in the fundamentals of synchrotron radiation techniques can check the classic review papers here [10,18,19].

The growing demand for safety and power in energy storage devices has led to the development of solid-state lithium-ion batteries (SSLBs) [24,25]. In-depth understandings of the material structure of the SSEs, electrodes, and their interfaces in terms of reaction and degradation mechanisms during synthesis, operation, and storage processes are essentially required. Taking into account the importance of the synchrotron technique, we present an overview of state-of-the-art application of the synchrotron X-ray technique in the characterization of solid-state battery materials. In particular, we highlight two aspects based on SSB challenges, including structural analysis of SSEs and the interfacial investigation between SSEs and electrode materials. As shown in Fig. 1, various synchrotron X-ray techniques will be discussed, such as X-ray diffraction (XRD), X-ray photoelectron spectroscopy (XPS), X-ray absorption spectroscopy (XAS), X-ray microscopy, to provide some basic guidelines to researchers.

Structural investigations of solid-state electrolytes (SSEs)

An ideal SSE should have the following fundamental properties: high ionic conductivity, high electronic resistance, wide electrochemical operating window, well chemical and thermal stability, low cost, environmental benignity for scale-up production, etc. [26,27]. Remarkable progress has been made in improving the properties mentioned above for inorganic and organic (polymer) SSEs. To reveal the structural and chemical information of SSEs, synchrotron X-ray diffraction (SXRD) is one of the most attractive methods. The working principle of SXRD is close to that of conventional XRDs using laboratory X-ray sources. However, the high resolution and intensity of the synchrotron beam enable the measurement of scattering from dilute phases or the analysis of residual stress [12,28]. Furthermore, X-ray crystal truncation rod scattering and X-ray reflectivity (XRR) techniques are able to detect the atomic- to nano-scale of thin films and interfaces [29,30]. In addition, synchrotron radiation has the unique advantages of enhancing signal strength and reducing test time, which enables the development of time-resolved XRD and in-situ/operando XRD in synchrotron beamlines. SXRD is able to determine the crystallographic information of materials, including lattice parameters of different phases, site occupancy, strain/stress, and microstructural information [10,12].

An early example of SXRD is reported by Kanno et al. that investigated the effect of oxygen substitution in sulfide-based SSEs $Li_{10}GeP_2S_{12}$ (LGPS) [31]. The LGPS has demonstrated high ionic conductivity of 1.2×10^{-2} S cm^{-1}. However, the LGPS has a very narrow stable electrochemical window and is not stable against Li metal, resulting in self-decomposition at low voltage triggered by Ge reduction. According to the result of the calculation, the chemical bonds between Ge/P–O are stron-

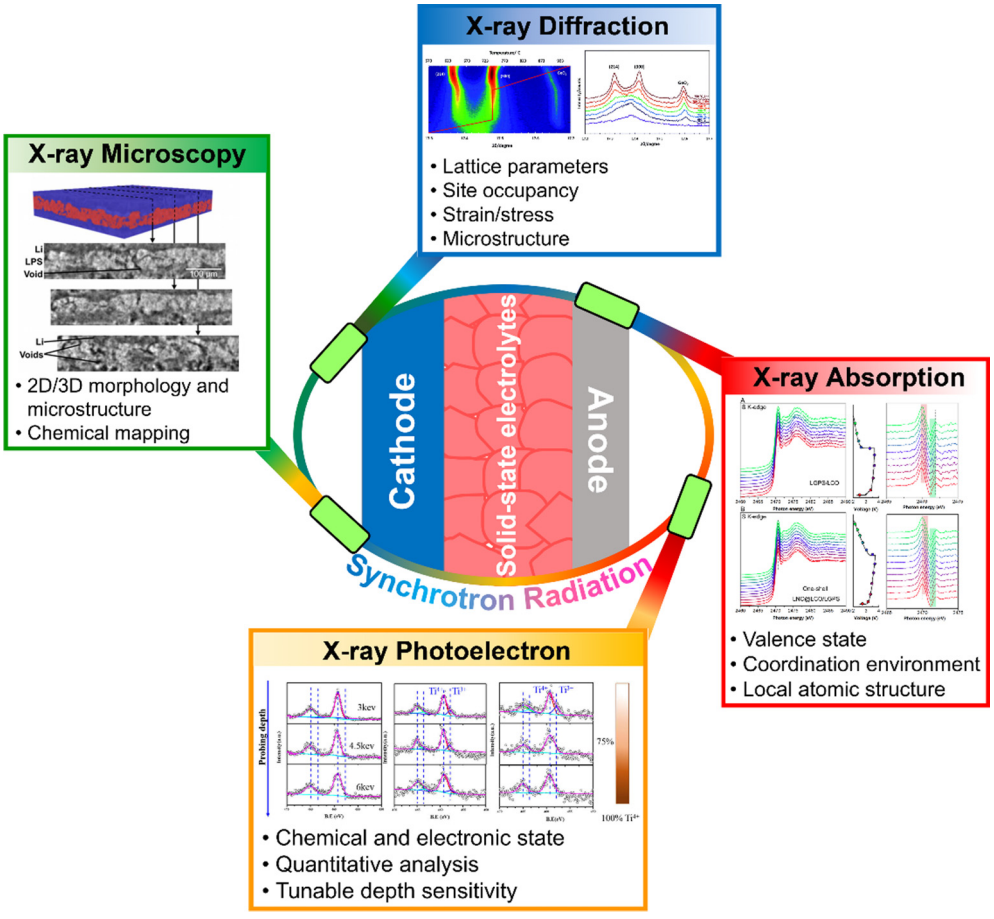

FIGURE 1

The schematic figure of synchrotron techniques in the study of SSBs [20]. Copyright 2016, Royal Society of Chemistry [21]. Copyright 2019, Wiley-VCH [22]. Copyright 2018, American Chemical Society [23]. Copyright 2018, The Electrochemical Society.

ger than those of Ge/P-S, the substitution of oxygen should, therefore, improve the thermodynamic stability. As shown in Fig. 2a, the Rietveld refinement results of SXRD show that the O atom prefers to occupy the specific site S (1) to substitute the S atom in PS_4 tetrahedral unit rather than the $(Ge/P)S_4$ or LiS_6 units. The partial substitution of S to O of $Li_{10}GeP_2S_{12-x}O_x$ ($0.3 \leq x \leq 0.6$) demonstrates the improvement of the electrochemical stability to Li metal and keep the high ionic conductivity within the range of 1.03×10^{-2} to 8.43×10^{-3} S cm^{-1} at 298 K [31]. Following this study, the doping effect of heteroatoms and the control of vacancy in SSBs were also studied via SXRD to reveal the lattice parameter change and phase evolution of SSEs in the relationship of chemical stability, ion migration pathway, and ionic conductivity [34–37]. In addition to the lattice parameters, SXRD is also capable of providing the microstructure information of the SSEs. Cheng et al. reported the effect of $Li_7La_3Zr_2O_{12}$ surface microstructure (LLZO) on the electrochemical performance with the use of high-resolution synchrotron polychromatic X-ray Laue microdiffraction [32]. The study examines the differences between large particles of LLZO (10 μm) and small particles of LLZO (1 μm) in terms of the distributions of grain orientation and misorientations of neighboring grains. As shown in Fig. 2b, the diffraction result indicates that there is no noticeable difference between large and small particles. For both samples, grain orientation is mostly random. The similar grain orientation distributions in the two cases, therefore, do not contribute to the observed differences in the electrochemical performance.

With the development of SSEs, researchers have discovered that the electrochemical properties of SSEs are closely related to the purity, uniformity, and chemical stability of the structure, which significantly depends on the choice of synthetic parameters. Therefore, in-situ SXRD characterization is applied to the study of the material structure evolution of the SSEs as a function of synthetic temperature and pressure. Adams et al. reported a detailed study of in-situ synchrotron XRD to rationalize and improve the synthesis process of NASICON-type $Li_{1+x}Al_xGe_{2-x}(PO_4)_3$ ceramics (LAGP) and to produce pure phase LAGP with effective Al doping [20]. As shown in Fig. 2c, the study showed that the sample began to crystallize at about 570 °C, while the effective Al incorporation into the LAGP structure requires prolonged heating up to 730 °C, with the obvious splitting of peaks (2 1 4) and (3 0 0) from the in-situ SXRD result. In addition, the study presents a complete in-situ SXRD analysis to provide a detailed scenario of the Al-doped LAGP phase transformation process. In the early stages of crystallization, the Al-poor LGP is the dominant phase, but gradually disappears with further heating of the sample, which gives a more homogeneous structure.

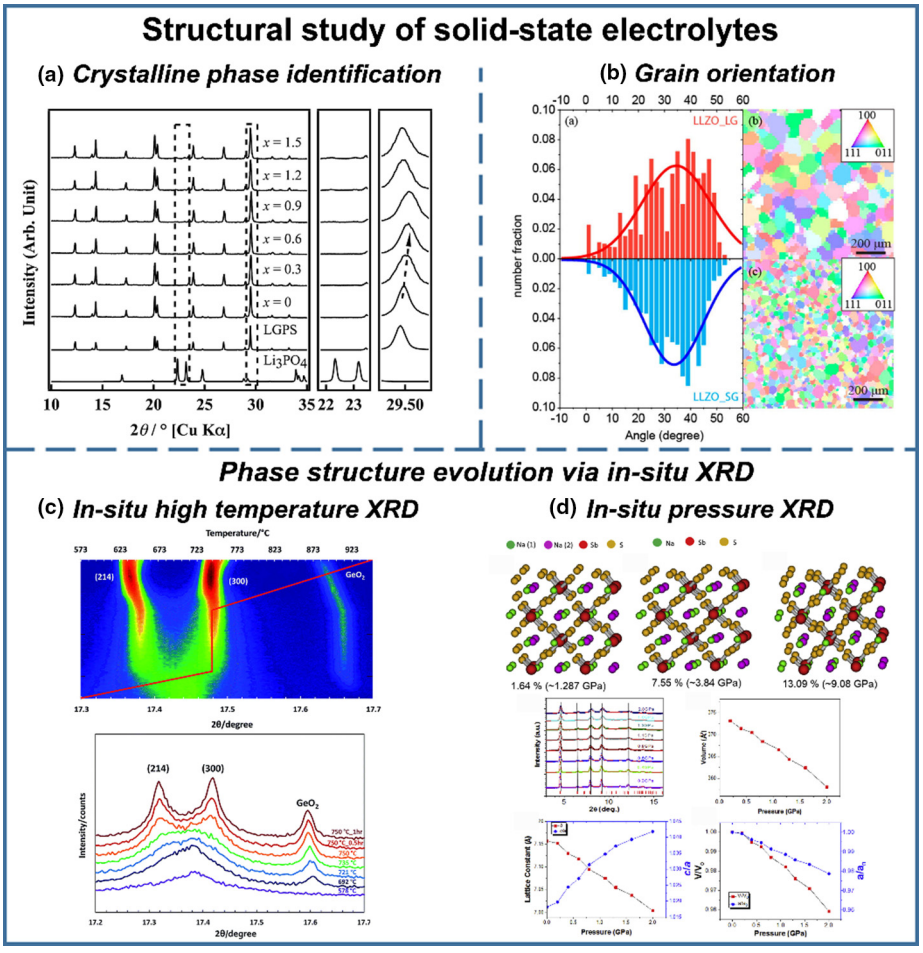

FIGURE 2

Various synchrotron-based XRD techniques applied in the characterization of SSEs. (a) Crystalline phase identification [31]. Copyright 2016, Elsevier. (b) Microstructure [32]. Copyright 2015, American Chemical Society. (c) Phase structure evolution via in-situ high temperature XRD [20]. Copyright 2016, Royal Society of Chemistry. (d) Phase structure evolution via in-situ pressure XRD [33]. Copyright 2018, Elsevier.

On the other hand, the heating of the sample at high temperatures (>950 °C) results in the extraction of Al from the outer shell of the LAGP particles and the formation of a germanium mullite $Al_{3-x}Ge_xO_{4.5+x/2}$ impurity phase. The impurity is then transformed to $AlPO_4$ at 300 °C during the cooling process. Based on the in-situ SXRD results, the authors suggest that the synthesis of LAGP should maintain the annealing temperature sufficiently below 950 °C to eliminate the impurity formation of germanium mullite and consequentially of $AlPO_4$. Following this study, further in situ SXRD studies of various SSEs, such as Al-doped $Li_7La_3Zr_2O_{12}$ (LLZO), atomic layer deposited (ALD) LLZO, and β-Li_3PS_4, were also reported to study the evolution of the phase transformation in related to the annealing temperatures [38–42]. In addition to the synthetic temperature, understanding the pressure effect on structure properties is just as important from a fundamental and practical point of view. In particular, most SSBs must be operated with extra pressure. On the basis of this consideration, Liang et al. have studied the effect of pressure on the structural evolution and conductivity of the Na_3SbS_4 superionic conductor via an in-situ SXRD from 0.2 to 2.0 GPa, as shown in Fig. 2d [33]. In situ SXRD patterns illustrate that diffraction peaks move to a larger 2θ degree and the peak widths gradually widen. Detailed refinement parameters indicate that the loading pressure increases the tetragonal distortion of the Na_3SbS_4 framework. By combining the in-situ Raman results, the study demonstrates that the tetragonal structure of Na_3SbS_4 is much more stable than the cubic structure, the phase transition of Na_3SbS_4 not being sensitive to pressure, which is beneficial for this solid electrolyte to maintain its stable performance in practical applications. Based on the limitation of space, other reported literature of synchrotron techniques applied in the structural studies of SSEs are summarized in Table 1.

Interfacial investigation in solid-state batteries

Significant improvements have been demonstrated during the development of highly ionic-conductive solid-state electrolytes in recent years. However, it should be noted that the integrity of SSEs applied in various battery systems still faces serious challenges due to the unstable interfacial behavior of SSBs [24,25,43]. The interface phenomenon causes a high impedance in the batteries and plays a critical role in the deterioration of battery performance, including (i) inferior solid–solid contact and large grain boundary between SSEs and electrode materials, (ii) formation of a lithium-deficient space charge layer between SSEs (e.g.,

TABLE 1

Summary of synchrotron techniques applied in the structural studies of SSEs.

SSEs	SR Techniques	Issue/challenges	Refs
$Li_{10}GeP_2S_{12-x}O_x$ ($0 \leq x \leq 0.9$))	XRD	Phase structural evolution of LGPS with O substitution	[31]
Li_2P2S_6	X-ray pair distribution function (PDF)	Crystalline structure confirmation	[34]
$Na_{10+x}Sn_{1+x}P_{2-x}S_{12}$ ($x = 0$, 0.2, 0.5, 0.8, 1)	XRD	Crystal structure confirmation and vacancy controlled Na^+	[36]
Al-doped $Li_7La_3Zr_2O_{12}$	XRD	Identify the Li^+/H^+ exchange related to the lattice parameter of LLZO	[37]
$Li_7La_3Zr_2O_{12}$	X-ray Laue microdiffraction	Grain orientations and boundary distributions	[32]
$(Li_{7-x}Al_{x/3})La_3Zr_2O_{12}$	In-situ XRD (temperature)	Thermal expansion as a function of Al content	[38]
$Li_{1+x}Al_xGe_{2-x}(PO_4)_3$	In-situ XRD (temperature)	Structural evolution of LAGP with heating and annealing process	[20]
ALD $Li_7La_3Zr_2O_{12}$	In-situ XRD (temperature)	Li loss at high-temperature annealing process	[39]
$Li_{1.5}Al_{0.5}Ge_{1.5}(PO_4)_3$	XRD (quasi in-situ temperature)	Identify the crystal structure with different temperature	[40]
Protic organic ionic plastic crystal $[DMEDAH_2][Tf]_2$ and PVDF	In-situ XRD (temperature)	Identify the crystal phase at first heating trace	[41]
β-Li_3PS_4	In-situ XRD (temperature)	Phase stability and phase transition	[42]
Na_3SbS_4	In-situ high pressure angle dispersive X-ray diffraction	Phase stability and phase transition	[33]
Al-doped $Li_7La_3Zr_2O_{12}$	Soft XAS	Air-stability of LLZO and distribution of Al and Li at the surface of LLZO	[32]

oxides and sulfides based SSEs) and cathode materials, (iii) side reactions and elemental diffusion to form interphases at the cathodic interface, (iv) growth of metal dendrites at the anodic interface, etc. [24,25,43–45]. Compared to the considerable work reported in the development of SSEs, the study on the interfacial behavior in SSBs remains insufficient. This is due to the challenges to reveal these interfacial behaviors, which include (1) local and heterogeneous reaction region, which requires high spatial resolution techniques with surface-sensitive or depth-resolved function to explore interesting reaction regions, (2) complex reaction process with formation of multiple by-products, which needs the techniques to identify specific elemental materials with local geometric/electronic structure, (3) rapid reaction process with transient intermediate states or species which needs in-situ or operando characterization to capture the detailed reaction manners [46–48]. Based on these requirements, many typical synchrotron-based X-ray techniques have been employed in the study of interfacial behaviors. For instance, high-energy XPS (HEXPS), X-ray absorption near edge structure (XANES), and extended X-ray absorption fine structure (EXAFS) are adopted to investigate the chemical/electrochemical interfacial reaction mechanisms of SSBs. X-ray imaging techniques, such as X-tomography, have been carried out to illustrate the microstructure change in the electrodes of SSBs.

Chemical/electrochemical interfacial reaction mechanisms

Sun et al. investigated the interfacial stability of NASICON type SSE LATP against Li metal with atomic layer deposition (ALD) Li_3PO_4 via synchrotron-based HEXPS, as shown in Fig. 3a [22]. XPS is one of the most versatile surface-sensitive techniques for the study of materials, which provides quantitative information of elemental compositions [10]. Compared to laboratory-scale XPS analysis, faster measurements and better resolution can be obtained with the use of bright synchrotron radiation. It is important to note that the tunable depth sensitivity at 2–50 nm can be achieved via tuning the photon energies, which provides the opportunity to perform non-destructive depth-resolved analysis [12,51]. In this study, three different probing depths for Ti 2p are chosen by tuning the excitation energies of 3000, 4500 and 6000 eV. After the LATP/Li symmetrical cell cycling, the bare LATP against the Li metal demonstrated the reduction of Ti from Ti^{4+} to Ti^{3+} in all HEXPS spectra. However, for LATP coated with Li_3PO_4 after cycling, the Ti^{3+} peak can only be observed at the very close surface, while the bulk region still retains the Ti^{4+} feature, indicating that ALD coating can prevent the Ti reduction for LATP.

In order to provide a detailed understanding and a more complete analysis of the interface behavior, recent research is to combine multi-synchrotron X-ray techniques in SSBs research. Miura et al. revealed the mechanism of the electrochemical reaction of $FePS_3$ in sulfide-based SSBs via ex-situ synchrotron-based XRD and XAS, as well as Raman and the first-principle calculations, as shown in Fig. 3b [49]. XAS is widely used in the investigation of the local geometric and electronic structure of materials [52,53]. A complete XAS spectrum is typically divided into two regions by the relative energy range to the absorption edge: X-ray absorption near-edge structure (XANES), which covers within 50 eV above the edge of absorption of an element, and the extended X-ray absorption fine-structure (EXAFS), which extends from about 50 eV above the edge to over 1000 eV [52–54]. XANES data provide quantitative or qualitative information on oxidation states, site symmetries and covalent bond strength of specific elements. EXAFS can be used to provide information on the local atomic structure of probed elements, such as interatomic distances, coordination number and chemical identity of the nearest neighbors via data simulation [10,16,55]. In the study of the $FePS_3$ reaction mechanism, the result of XRD and Raman shows that $FePS_3$ maintains the $P_2S_6^{4-}$ unit during the discharge–charge process, while the crystalline structure of $FePS_3$ turns to be weak during the charging process. In addition, the

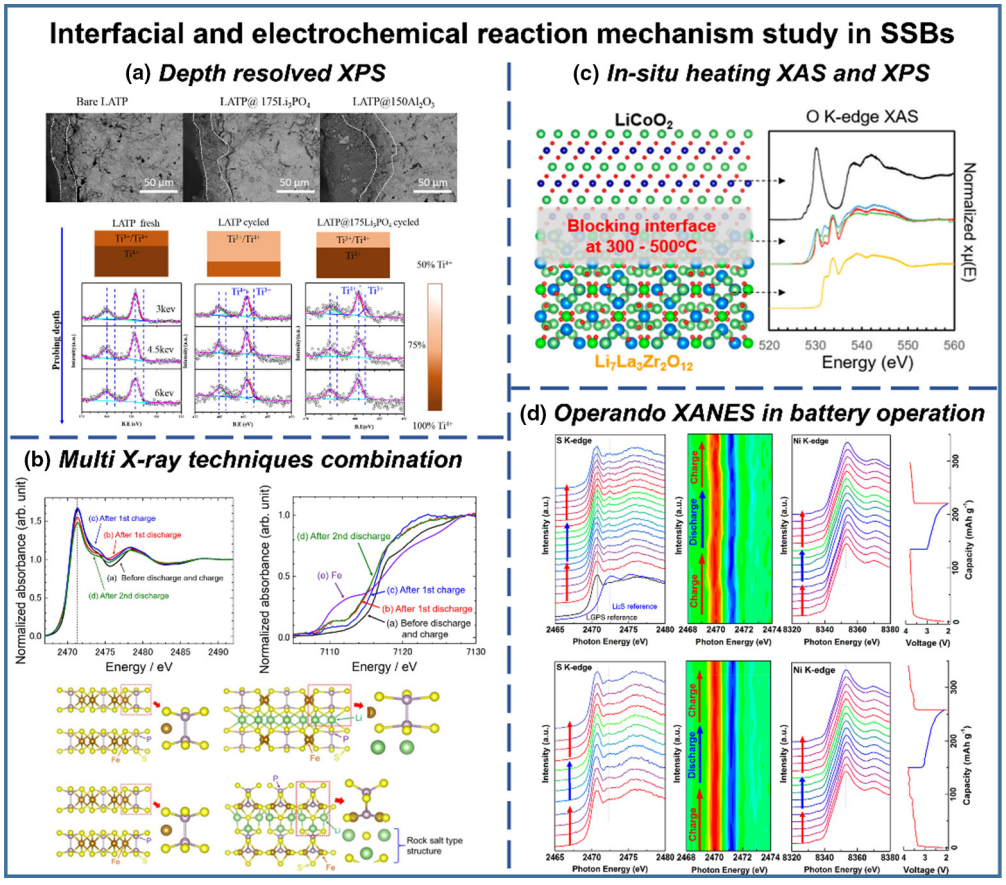

FIGURE 3

Synchrotron X-ray techniques in the study of interfacial reaction mechanisms in SSBs. (a) Depth-resolved XPS [22]. Copyright 2018, American Chemical Society. (b) Multi X-ray techniques [49]. Copyright 2018, The Electrochemical Society. (c) In-situ high-temperature XAS and XPS [50], Copyright 2018, American Chemical Society. (d) Operando XANES [9]. Copyright 2019, American Chemical Society.

result of Fe K-edge and S K-edge XANES indicated that the Fe element participates in the redox process from the first discharge process and the S element may also join the electrochemical process after the first charge cycle onwards. Based on the obtained experimental results, the study simulated the potential structure models and the reaction pathway of $FePS_3$ computationally. Two types of $FePS_3$ and $Li_{1.5}FePS_3$ (trigonal and octahedral coordination geometries) are constructed. Based on the calculated equilibrium voltage of the lithium intercalation reaction and density-of-states (DOSs) of the established $FePS_3$ modeling structures, the study proposed a complete transition process from $FePS_3$ to $Li_{1.5}$-$FePS_3$. The study highlights the combination of multi-synchrotron X-ray techniques with computational chemistry strategies, which can be applied in many studies of undisclosed reaction mechanisms. Furthermore, many other studies have also employed X-ray techniques combined with multiple physical characterizations to investigate the interface behaviors in SSBs, such as X-ray CTR for thin film surface/interface crystalline characterization [45], X-ray tools combined with transmission electron microscopy (TEM) and electron energy loss spectroscopy (EELS) for material microstructure characterization [9,22]. Based on the limited space, we will not give details for all the studies and have summarized the general information in Table 2.

To further reveal the interfacial behavior of SSBs during dynamic processes, in-situ and operando X-ray techniques have also been established. As shown in Fig. 3c, Yildiz et al. used in-situ synchrotron-based XRD, XPS, and XAS to provide a comprehensive understanding of the structure, chemistry, and charge-transfer resistance of the interface between LLZO and $LiCoO_2$ (LCO) in terms of annealing temperature [50]. Firstly, the study performed synchrotron-based XPS and XAS to investigate the depth of reaction in the interfacial region, as well as the corresponding oxidation state of the electrodes and SSEs. The XAS spectra of Co K-edge, Co L-edge and O K-edge of LCO/LLZO samples indicate that the annealing process induces the oxidation of Co element while the decomposition of LLZO occurs at the interface. In addition, the study carried out in-situ O K-edge XAS and in-situ C 1s XPS during the heating process in the oxygen atmosphere to unravel the decomposition process of surface impurity Li_2CO_3. Finally, by combining synchrotron XRD and EXAFS, the study demonstrated the formation of the secondary phase of La–Co–O at the interface of LCO and LLZO at the depth of 20 nm after annealing at 500 °C. These results indicate that synthetic conditions at lower temperatures, short time scales, and in CO_2-free environments are highly desirable to obtain rapid Li^+ transfer at ceramic cathode-electrolyte

TABLE 2

Summary of synchrotron techniques applied in the study of the interfacial reaction in SSBs.

Electrode/SSE materials	Methods	Issue/challenges	Refs
Li_3PS_4/acetylene black carbon	XPS + XANES	Structural and electronic-state changes of a sulfide solid electrolyte during the Li deinsertion–insertion	[46]
$LiCoO_2$/80Li_2S·20P_2S_5 and $LiCoO_2$/Li_3PO_4/80Li_2S·20P_2S_5	Depth-resolved XAS (XANES and EXAFS)	Interface reactions during the discharge–charge process between LCO and LPS with/without coating	[47]
$(Li_2S)_x(P_2S_5)_{100-x}$ glasses ($50 < x < 80$)	XANES + XPS	Compositional depolymerization of interconnected PS_4 tetrahedra in $(Li_2S)_x(P_2S_5)_{100-x}$ glasses	[48]
$FePS_3$/75Li_2S·25P_2S_5	XRD + XANES + Raman + Simulation	Reaction mechanism of $FePS_3$ using sulfide-based solid electrolytes	[49]
$LiFePO_4$/$Li_{3+x}P_{1-x}Si_xO_4$	XANES + XRD + NMR	Identify the interface reaction between LFP and LPSO	[44]
NASICON/Li metal anode	HEXPS + TEM	Interface reaction of NASICON solid electrolyte against Li metal with ALD coating	[22]
$LiCoO_2$/Li_3PO_4	X-ray crystal truncation rod scattering	Crystal structure of surface cathode effect on the interface resistance	[45]
$LiCoO_2$/$Li_7La_3Zr_2O_{12}$	In-situ XAS + XRD + in-situ XPS at different temperature	Interface stability between LCO and LLZO	[50]]
$LiCoO_2$/$Li_{10}GeP_2S_{12}$	Operando XANES + XPS	Interface stability between LCO and LGPS	[21]
NMC811//$Li_{10}GeP_2S_{12}$	Operando XANES + TEM	Interfacial reaction and microstructure evolution	[9]

interfaces. In sulfide electrolyte based SSBs, Sun et al. employed operando XANES study to understand the interfacial reaction mechanisms between various cathode materials and sulfide SSEs [9,21]. One of the study is to unravel the interfacial behavior between the Ni-rich layered $LiNi_{0.8}Mn_{0.1}Co_{0.1}O_2$ (NMC811) cathodes and $Li_{10}GeP_2S_{12}$ (LGPS) SSEs [9]. As shown in operando S K-edge spectra with first derivative mapping (Fig. 3d), LGPS SSE with bare NMC811 is unstable in the electrochemical process. LGPS presents a metastable intermediate state at the initial charging process and some of the LGPSs are decomposed to form a Li_2S impurity phase afterwards. Furthermore, combined with TEM characterization, the study demonstrates the microstructure degradation of NMC811 from the surface to bulk during cycling, leading to the microstructural cracks at the surface of cathode particles, surficial transition metal reduction of cathodes, and phase evolution from the layered to rock-salt structure. The study also employed atomic layer deposition (ALD) for cathodes to further investigate the cathodic interface stability. The synthesized ALD $LiNbO_x$ coating helps to protect the integrity of the NMC811 cathode and stabilize the interface with LGPS SSEs. This study expands the understanding of the interface mechanism of inorganic based SSBs and demonstrates the potential of operando synchrotron based characterization studies to probe the highly reactive intermediate states and unravel the complex reaction mechanisms of energy materials. It should be noted that the coin-cell operando battery configuration poses many challenges during the experiment and operation and needs to be further developed in the future.

Microstructure visualization of electrodes in SSBs

The structure of the electrodes in the SSBs faces more severe challenges than in the liquid-based batteries [24,25,27]. For example, intimate solid–solid contact between electrodes and solid-state electrolytes is critical to form an effective ionic conductive pathway. However, the volume change of cathode materials during the charge–discharge process, such as Ni-rich layered structure cathodes, causes the cathode materials to crack and separate from the SSEs, making it difficult to maintain intimate contact with the SSEs and directly deteriorates SSB performance. In addition, from the side of the metal anode, such as Li metal anodes, the heterogeneous distribution of electrons at the interface between the SSEs and the anodes aggravates the non-uniform diffusion of lithium ions, as well as the formation of Li dendrite, which seriously endangers the safety of SSBs. Therefore, in-depth understanding and optimization of the microstructure in SSBs are essential in the design of safe and high-performance SSBs. The development of synchrotron X-ray microscopes allows direct visualization of battery materials in a non-invasive manner [12]. Especially for X-ray tomography, the 3D structure of the sample can be reconstructed in real space, allowing visualization and quantification of 3D morphological information, such as spatial fractions, volume/contact area, and particle cracking of electrodes [12,16,56,57]. Zhu et al. used ex-situ synchrotron transmission X-ray microscopy tomography with a resolution of 52.3 nm to investigate the 3D morphology of the solid state electrode pellet with a mixture of $Li(Ni_{1/3}Mn_{1/3}Co_{1/3})O_2$, $Li_{1.3}Ti_{1.7}Al_{0.3}(PO_4)_3$ and Super-P carbon, as shown in Fig. 4a [58]. The study quantitatively analyzed the volume fraction and geometric properties of the electrodes in terms of pressure pressed on the electrode pellets. The results of the tomography found that even increase to a large pressure (1300 psi), there is still a fraction of space volume in the electrode and the contact area of cathodes with electrolytes is limited, which significantly affects the transport of lithium ions in the electrode.

X-ray imaging techniques are also able to study the dynamics of 3D morphological evolution with in-situ/operando configuration. For example, Sun et al. combined synchrotron operando X-ray tomography and energy dispersive diffraction to investigate the morphological and compositional evolution of the interface between the Li-In anode and $Li_{10}SnP_2S_{12}$ SSE in all-solid-state Li-S batteries [59]. As shown in Fig. 4b, the study designed a modified Swagelok cell as an operando cell configuration and the resolution of the X-ray tomography in this study is 2.5 μm. By combining the results of the operando X-ray tomography and energy dispersive diffraction, the study demonstrated the volume change of Li–In anode and proposed that the change in volume causes the build-up/release of the strain/stress in the layer of electrodes that can further change the mechanical structure of the

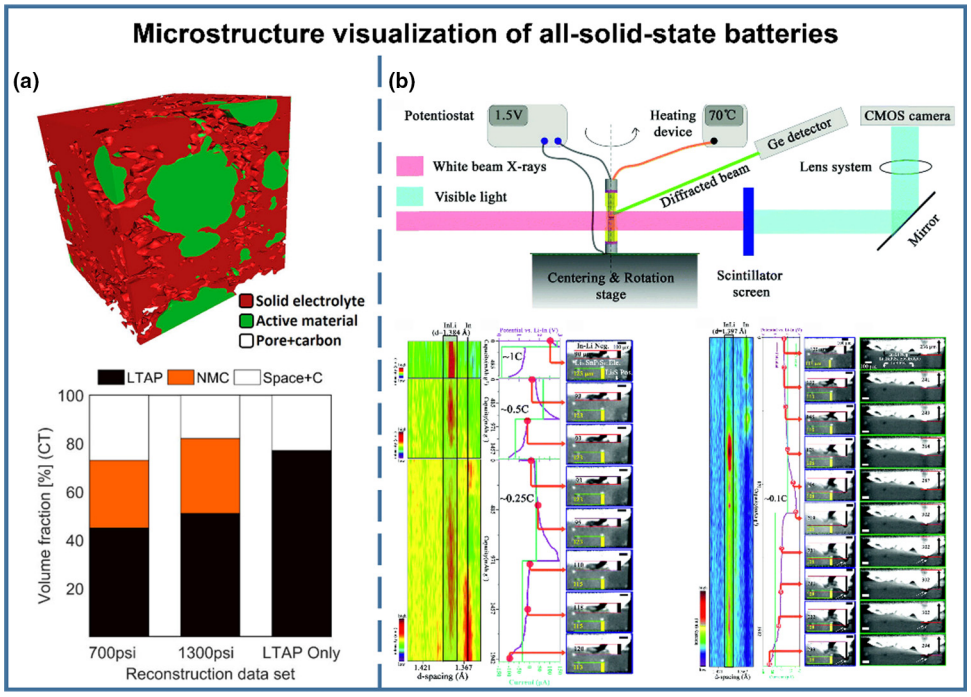

FIGURE 4

X-ray tomography techniques applied in SSBs. (a) Ex-situ transmission X-ray microscopy tomography applied in the electrode microstructure study [58]. Copyright 2018, American Chemical Society. (b) Operando X-ray tomography study in all-solid-state Li-S batteries [59]. Copyright 2018, Royal Society of Chemistry.

TABLE 3

Summary of synchrotron techniques in the study of microstructure visualization in SSBs.

Electrode structure	SR Techniques	Issues/Challenges	Refs
$Li(Ni_{1/3}Mn_{1/3}Co_{1/3})O_2/Li_{1.3}Ti_{1.7}Al_{0.3}(PO_4)_3$/ Super-P carbon electrode	Transmission X ray microscopy tomography (Resolution 58.2 nm)	Electrode/SSE contact issues	[58]
LLZO/Li interface	X-ray tomography (Resolution 500 μm)	Pore connectivity and propagation in LLZO for Li dendrite growth	[57]
Li/β-Li_3PS_4/Li	In-situ X-ray tomography (Resolution 1.3 μm)	The formation and propagation of Li metal features within SSEs	[23]
Li-In/LSPS/Li_2S all-solid-state Li-S batteries	Operando X-ray tomography (Resolution 2.5 μm)	Record the morphological and compositional evolution at the anodic interface during battery cycling.	[59]
$LiNi_{0.8}Co_{0.15}Al_{0.05}O_2$/PEO/Li	2D/3D full-field (FF) transmission X-ray microscopy (Resolution tens nm)	Morphology and state of charge inhomogeneity within secondary NCA particles in solid polymer batteries	[60]

electrolyte/electrode interface and weaken the connection between them. In addition to the Li–In anode, Seitzman et al. also reported the migration of the Li anode to the SSE sulfide (β-Li_3PS_4) in the symmetric Li/β-Li_3PS_4 cell using the in-situ X-ray tomography technique [23]. It should be noted that the application of X-ray imaging techniques in SSBs is still at a very early stage and it is believed that these techniques would contribute greatly to the comprehensive understanding of microstructure visualization and the heterogeneous distribution of the chemical structure in the SSBs. Other X-ray microscopy studies in SSBs are summarized in Table 3.

Solid-state NMR spectroscopy

NMR signals originate from the interaction between the external magnetic field and the studied nuclei. This principle fundamentally determines that NMR is possible to explore every atomic site in a material. In recent years, solid-state NMR (SS NMR), with the demonstrated ability to detect the local structure and ionic dynamics of specific nuclei, has become an indispensable characterization method for analyzing ionic movements and local structure at the atomic level [11,61]. With the application of various NMR methods, abundant structural and dynamic information can be accessed [62,63]. These methods include (i) magic angle spinning (MAS) NMR [64,65], which provides the precise local structure of the solid-state electrolyte [66], as well as the identification of interfacial species; (ii) the pulsed-field gradient (PFG) NMR [67] and the NMR relaxation time measurement [68,69], which are sensitive to ionic movement at different time/length scales. For example, the time scale measured by the PFG NMR technique is 10^{-2} to 10^{-1} s, corresponding to a

length scale of approximately 1 μm. NMR relaxation methods, which include the spin–lattice relaxation (T_1), spin–spin relaxation (T_2) and spin–lattice relaxation in the rotating frame ($T_{1\rho}$) [70], are very sensitive to measure single transitions of the $10^{-10} \sim 10^{-3}$ s time scale (the specific time scales of T_1, T_2 and $T_{1\rho}$ are illustrated in Fig. 5). In addition, the line width of NMR signals, which is inversely related to T_2, also can be used to qualitative analysis of ion motion in the materials [63]; (iii) two-dimensional exchange spectroscopy (2D EXSY) NMR [71,72], which can be used to explore the transport path and rates of two different chemical sites. These two chemical sites can be two lithium sites in a single material, but also of different materials (such as cathode and solid state electrolyte) [73], which can investigate the ionic transport path within SSEs, and at the interface; (iv) magnetic resonance imaging (MRI) techniques, which have the capability for spatial resolution, can provide information on the interfacial microstructure, morphology and elemental distribution. Fig. 5 summarizes the diverse information, including site occupancy, ionic movement, interface products, and the transport pathways, provided by the SS NMR methods.

The recent application of SS NMR in SSBs research is summarized in Tables 4 and 5, which demonstrate the compatibility of SS NMR with almost all solid-state electrolytes. In particular, the unique advantages of SS NMR in the study of transport properties of carriers on an atomic scale would be highlighted in the following discussion, which illustrates two aspects. The first is the ionic movement within the solid-state electrolyte and the second is about the interface problems in the SSBs, which are supposed to provide an in-depth understanding of the ionic transport in solid-state electrolytes, as well as in the interface. For a detailed introduction of some basics of NMR, we recommend readers several excellent reviews and monographs [11,75–77].

Structural and dynamical investigation

Understanding the structure of SSEs and corresponding ionic transport properties, including transport rate and transport pathway, from a microscopic perspective, are key issues that can provide guidelines for designing solid electrolytes with superior performance. Ionic conductivity is one of the most important parameters that determine the performance of the solid-state electrolyte, which is always regulated by the element doping. To better understand the doping mechanism and the corresponding occupancy of the site, high-resolution magic angle spinning (MAS) NMR is considered a powerful method. A typical example is a study of garnet-type electrolytes $Li_7La_3Zr_2O_{12}$ (LLZO), which have received growing attention since their discovery in 2007 [96]. The LLZO cubic phase has two orders of magnitude of ionic conductivity higher than the LLZO tetragonal phase. It is reported that doping with Ga and Al could stabilize the cubic phase, thus obtaining high ionic conductivity [97,98], while there is still some controversy over its stability mechanism. Based on this problem, ^{27}Al and ^{71}Ga MAS NMR spectra were acquired in ultra-high magnetic fields, which revealed that Al and Ga simultaneously occupy the 24 d and 96 h sites of the LLZO network. This result demonstrates that the presence of Al and Ga at Li sites is responsible for stabilizing the cubic phase of LLZO, rather than Al and Ga exist in the grain boundary. In general, doping the heterovalent element would cause a charge imbalance that would lead to a redistribution of lithium in LLZO. For example, replacing Zr^{4+} with W^{5+} would decrease the total amount of lithium ions in LLZO. By T_1-filtered ^6Li MAS NMR, Yang et al. distinguished the three lithium sites for the first time in W-doped LLZO, as shown in Fig. 6a. They found that the charge imbalance caused by the doping of W was compensated by reducing the occupancy of lithium-ion at sites of 48 g [72]. Similar to LLZO, the doping mechanism of other SSEs, such as LATP and Li_4SiO_4–Li_3PO_4, has also been investigated by MAS NMR [82,99]. In addition to site occupancy, dynamic NMR methods are indispensable for studying ionic motion in the solid-state electrolytes. The effects of Ga/Al doping on the Li^+ transport rate in LLZO are investigated qualitatively by the line width of the ^7Li NMR signals as the function of temperature [70]. The line width of the ^7Li signal in $Li_7La_3Zr_2O_{12}$ began to narrow at 280 K, while the Ga/Al doping $Li_7La_3Zr_2O_{12}$ narrowed at 180 K. The lower narrowing temperature of the line width indicates a faster ionic movement in the Ga/Al doped $Li_7La_3Zr_2O_{12}$. The effect of Al doping on ionic mobility in $Li_{1+x}Al_xTi_{2-x}(PO_4)_3$ $(0 \leq x \leq 1.0)$ was characterized by the measurement of the relaxation time $T_{1\rho}$ of ^7Li, as shown in Fig. 6b [81]. The results indicate that when the ionic jump rates of Li^+ of all materials are equal to 4×10^5 s^{-1}, materials with doping amount of Al of 0.35 and 0.5 require the lowest temperature, demonstrating the higher ionic mobility of the two materials. Therefore, the optimal amount of doping of Al is determined between 0.35 and 0.5 by this method. In addition to the transport rate within the SSEs particles, the transport rate at the grain boundary is considered the slowest in long-range diffusion, which limits the total ionic conductivity [27]. Lotsch et al. performed ^7Li PFG NMR with short and long diffusion time to investigate the ionic movement of the SSEs at the bulk and grain boundary respectively [87]. They observed the presence of an amorphous impurity phase that inhibits the inter-grain conductivity, thus providing the poor total conductivity. Recently, also in the solid sulfide electrolyte, Ganapathy et al. used ^6Li 2D EXSY to quantitatively study ionic movement at the grain boundary [71]. As shown in Fig. 6c, the results demonstrate the comparable value of the activation energy at the grain boundary (0.27 ev) and the bulk phase (~0.20 ev). They considered that in the Li_6PS_5X system (X = Br, Cl), the grain boundary is not the rate-limiting step of lithium-ion transport due to the high ductility of the thiophosphates. Such an NMR method makes it possible to quantitatively study the ionic movement in the grain boundaries, which can be extended to other types of solid electrolytes in future research.

With the study of solid-state electrolytes, more and more research work focused on the transport pathways of carriers, which together with the transport rate determine ionic conductivity. Therefore, various NMR techniques were developed and employed to study ionic transport pathways. Taking the $Li_{10}GeP_2S_{12}$ (LGPS) as a model, Liang et al. used the temperature-dependent ^7Li Spin Alignment Echo (SAE) experiment, for the first time, experimentally observed the two different transport pathways in LGPS [90]. In the low-temperature regime, Li^+ transport only along the c axis. When the temperature is evaluated above 257 K, Li_4 sites begin to participate in the transport of lithium ions, which triggers another transport

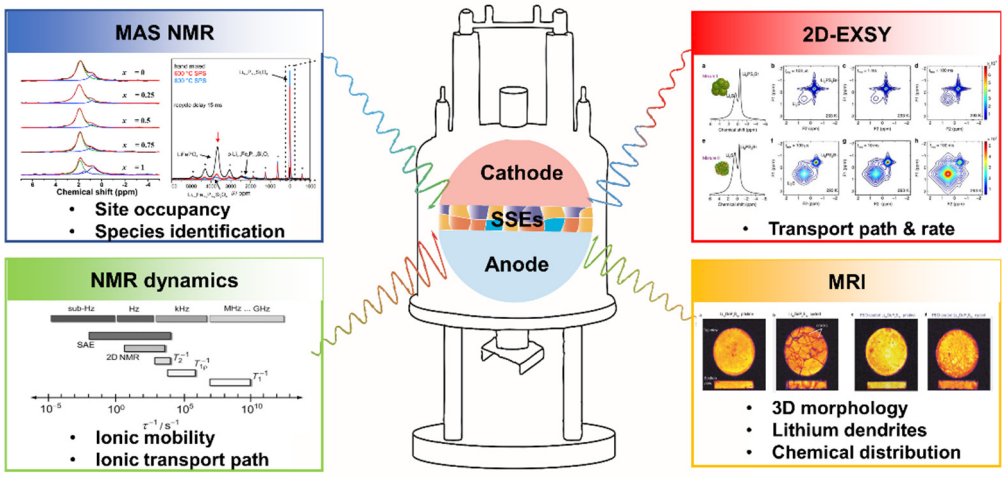

FIGURE 5

Summary of solid nuclear magnetic methods in solid-state battery research. Copyright 2014, Royal Society of Chemistry [64]. Copyright 2018, American Chemical Society [44]. Copyright 2018, Nature Publishing House [73]. Copyright 2012, American Chemical Society [63]. Copyright 2018, American Chemical Society [74].

TABLE 4

Summary of the application of SS NMR in solid state electrolyte research.

	SSEs	NMR Methods	Main conclusions	Refs
Site Occupancy	$Li_5La_3Nb_2O_{12}$	^{6}Li–^{7}Li CPMAS	Li_1 and Li_2 sites were resolved by NMR	[78]
	$Li_7La_3Zr_2O_{12}$	^{7}Li T_1-suppress MAS	Li_3 site was found for the first time by NMR	[72]
	$Li_{7-x}Al_{x/3}La_3Zr_2O_{12}$	^{27}Al and ^{71}Ga MAS NMR	Al and Ga occupy the Li_1 and Li_2 sites and may obstruct the transport path	[66]
	$Li_{7-x}Al_{x/3}La_3Zr_2O_{12}$	^{27}Al MQ MAS	Identification of impurities during the synthesis process	[79]
	$Li_{1+x}Ti_{2-x}Al_x(PO_4)_3$	^{27}Al MAS	Identify the site occupancy of Al	[80–83]
	$Li_{1+x}Ti_{2-x}Sc_x(PO_4)_3$	^{45}Sc MAS	Identify the site occupancy of Sc and Sc-bearing impurities	[84]
	$Li_{1+x}Ti_{2-x}Al_x(PO_4)_3$	^{31}P MAS	The local environment of P varies with the number of surrounding Ti and Al	[82,85]
	$Na_{3-y}PS_{4-x}Cl_x$	^{23}Na MAS	Identify the site occupancy of sodium	[86]
Transport rate in SSEs	Li_7SiPS_8	^{7}Li PFG NMR	Effect of the impurities at the grain boundary on the overall ionic conductivity	[87]
	$Li_{10}GeP_2S_{12}$	^{7}Li T_1, T_2, Line width, PFG	Ionic motion at different lengths/time scales	[67]
	$Li_{3.75}Si_{0.75}P_{0.25}O_4$ $Li_{3.5}Si_{0.5}P_{0.5}O_4$ $Li_{3.25}Si_{0.25}P_{0.75}O_4$	^{7}Li T_1	The ionic mobility with different Si/P ratio	[88]
	Li_6PS_5Cl	^{7}Li T_1	Effect of synthetic methods on ionic motion	[69]
	Li_6PS_5Br	^{7}Li T_1, $T_{1\rho}$	Comparison of ionic motion between grain boundaries and bulk phases	[68]
	$Na_3Sc_xZr_{2-x}(SiO_4)_{2-x}(PO_4)_{1-x}$	^{23}*Na* T_1	Effect of Sc doping on the ionic motion of sodium ions	[65]
	Na_3PS_4	^{23}*Na* T_1	Ionic motion in the Na_3PS_4 polymorph (cubic and tetragonal)	[89]
	Li_6PS_5X (X = Cl, Br)	^{7}Li 2D EXSY	A quantitative study of ionic motion at grain boundaries	[71]
Transport pathways in SSEs	$Li_7La_3Zr_2O_{12}$	^{7}Li 2D-EXSY	Confirm the transport path in garnet-type SSE along the loop of Li_1–Li_3–Li_2–Li_3–Li_1	[72]
	$Li_{10}GeP_2S_{12}$	^{7}Li SAE	Transport mechanism in LGPS 2D (below 257 K), 3D (above 257 K)	[90]
	$Na_3Zr_2Si_2PO_{12}$	^{23}Na T_1	Reveal the transport path in $Na_3Zr_2Si_2PO_{12}$	[91]
	$Li_7La_3Zr_2O_{12}$-PEO	^{6}Li replace ^{7}Li	Reveal the transport path in PEO-$Li_7La_3Zr_2O_{12}$ composite electrolyte	[92]
	$Na_9Al(MoO_4)_6$	^{23}Na T_1	Reveal the transport mechanism of sodium ions in terms of temperature	[93]

path in the ab plane. Therefore, the general transport path at room temperature (greater than 257 K) appears as a three-dimensional diffusion that leads to the high ionic conductivity of LGPS. Compared to SAE NMR, 2D EXSY NMR is a more intuitive way to observe the lithium-ion transport path. Wang et al performed ^{6}Li 2D EXSY in LLWZO, whereby they observed the

TABLE 5

A summary of the application of SS NMR in the study of the interface in the solid-state battery.

	Interface	Method	Interfacial investigation	Refs
Interfacial species	$LiFePO_4/Li_{3+x}P_{1-x}Si_xO_4$	^{31}P MAS	Identify the interfacial species caused by the migration of iron ions	[44]
	$Li/Li_{6.5}La_3Zr_{1.5}Ta_{0.5}O_{12}$	^{7}Li 1D MRI	Record the evolution of lithium dendrite	[94]
	$Li/Li_{6.55}Ga_{0.15}La_3Zr_2O_{12}$	^{7}Li Static NMR	Lithium dendrite	[95]
	$Li/Li_{10}GeP_2S_{12}$	^{7}Li 3D MRI	Uneven distribution of Li ions at the interface after electrochemical cycling	[74]
	Li_2S/Li_6PS_5Br	^{7}Li 2D-EXSY	Determine the transport rate at the interface of Li_2S–Li_6PS_5Br	[73]

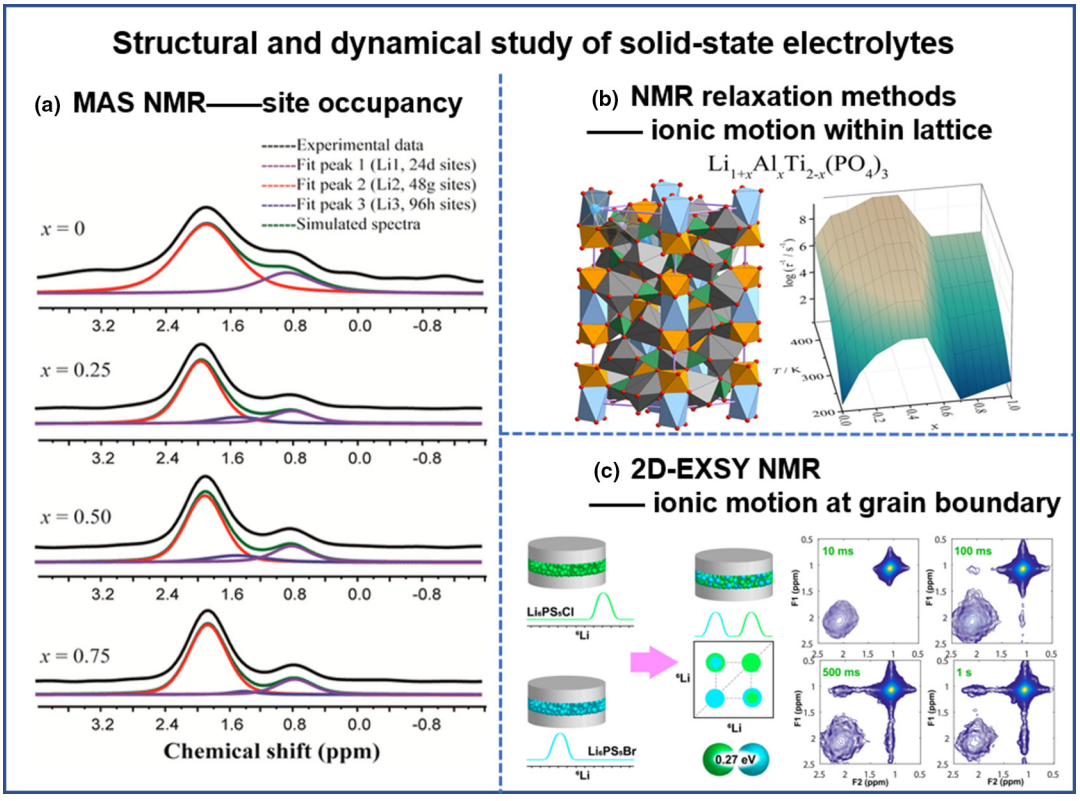

FIGURE 6

SS NMR in the study of structure and dynamics of solid-state electrolytes. (a) Site occupancy. Copyright 2015, American Chemical Society [72]. (b) Ionic motion in solid-state electrolytes, Copyright 2016, American Chemical Society [81] and (c) at the grain boundary. Copyright 2019, American Chemical Society [71].

cross peak between Li_3 sites and Li_1 sites [72]. This result directly demonstrates that the lithium-ion transport path in $Li_7La_3Zr_2O_{12}$ is a long cycle of Li_1–Li_3–Li_2–Li_3–Li_1, during which the mobility of Li_2 is slowest. Therefore, the transport of lithium ions at the Li_2 sites is considered a rate-determining step that limits the ionic conductivity. In addition to inorganic SSEs, the transport path in composite SSEs that composed of inorganic SSEs and organic polymers is still obscure. Based on this problem, Hu et al. built $^{6}Li||Li_7La_3Zr_2O_{12}/$ PEO $||\,^{6}Li$ symmetric cells to monitor the ^{6}Li transport path during cycling in the composite electrolyte. With the increase in the content of $Li_7La_3Zr_2O_{12}$, the ionic conductivity of the composite electrolyte decreases and the transport pathway of ^{6}Li gradually changed from PEO to $Li_7La_3Zr_2O_{12}$. When 50% (wt%) of $Li_7La_3Zr_2O_{12}$ was added, the transport path only passed the loose particles of $Li_7La_3Zr_2O_{12}$, which deteriorate the total ionic conductivity. After this study, several composite electrolytes with different recipes have been used to investigate the transport pathways [92,100,101].

Interfacial investigation in solid-state batteries

In recent years, the ionic conductivity of solid-state electrolytes has been greatly improved. However, the incompatibility and chemical/electrochemical instability of the electrode/electrolyte interface limit the practical application of SSBs [4]. Despite much attention to mitigate poor performance, understanding of the root causes that explain poor performance is limited, which challenged by the difficulty of investigating the chemical and physical properties of the interface due to the complex and transient reaction [7]. This has motivated the use and development of some advanced NMR techniques to investigate the interfacial reactions of SSBs, such as MAS, 2D-EXSY and MRI.

In SSBs, the cathode materials were frequently mixed with SSEs and followed by heat treatment as a composite cathode to improve compatibility between the cathode and the SSEs. Grey and co-workers used ^{31}P MAS NMR spectra to study the composition of the composite cathode consisting of the $LiFePO_4$ cathode and the $Li_{3+x}P_{1-x}Si_xO_4$ solid-state electrolyte [44]. The

specie $Li_{3-z}Fe_zP_{1-z}Si_zO_4$ appears after SPS (Spark Plasma Sintering), which caused by the transport of iron ions from $LiFePO_4$ to $Li_{3+x}P_{1-x}Si_xO_4$. This result indicates that heat treatment can affect the composition of the composite cathode due to ion migration. In addition to the composition, heat treatment also affects the transport properties of lithium ions at the cathode/SSE interface. Yu and co-workers performed ^{7}Li 2D EXSY to quantitatively illustrate the transport rate at the interface between the Li_2S cathode and Li_6PS_5Br SSE under different sample preparation conditions [73]. As shown in Fig. 7a, the results indicate that sample preparation, such as nanosizing and ball milling, can accelerate the spontaneous exchange of lithium ions at the cathode / SSE interface. However, the electrochemical cycle can destroy this exchange. It is worth noting that these two previous works mainly focus on the interfacial issues during the preparation process other than the electrochemical cycle process. In the near future, In-situ NMR technique is expected to be useful when studying the ion transport process in working conditions.

In SSBs, the anode/SSE interface can be classified into three types, (i) the kinetically stable interface, such as Li/LLZO (ii) continuously reactive interface, such as Li/LGPS (iii) self-limiting reactive interface, such as Li/Li_3ClO [4]. For the kinetically stable interface, the main problem is the growth of lithium dendrites. Benefitted from the different chemical shifts between bulk and dendritic lithium metal, Aguesse et al. observed the signal of lithium dendrites in $Li_7La_3Zr_2O_{12}$ using static solid-state NMR [95]. Recently, as shown in Fig. 7b, Grey and co-workers used 1D in-situ ^{7}Li MRI to monitor the growth of lithium dendrites in $Li_7La_3Zr_2O_{12}$ [102]. With the ability of in-situ MRI to study the dynamic evolution of the interface, the entire process of the lithium dendrite is completely observed from the beginning of the surface growth to the connection of the two electrodes. This method can be further used to explore the relationship between the growth rate of lithium dendrite with a current density, as well as the thickness of the SSE pellet in the future, and is expected to reveal the key factors affecting the formation and the growth of lithium dendrites. For a continuously reactive interface, the main problem is the constant increase in interfacial impedance. Hu et al. with the help of 3D MRI techniques, monitored the distribution of lithium at the Li/LGPS interface during cycling, as shown in Fig. 7c [74]. The 3D image clearly showed the uneven distribution of lithium ions at the Li/LGPS interface after cycling, which was considered as the direct origin of the continuous increase in interfacial resistance. However, the PEO-coated LGPS can maintain a relatively uniform distribution of lithium ions, thus achieving a small interfacial impedance. It is worth noting that the current temporal/spatial resolution of MRI should be further improved, which requires a larger magnetic field gradient or a more advanced NMR pulse technique.

Neutron scattering

Over the past decade, neutron scattering has received increasing attention as a powerful tool for studying materials and battery systems. This application of neutron scattering was further driven by the commissioning of the spallation neutron source (SNS) at the Oak Ridge National Laboratory in 2006 [103]. Today, SNS has become the world's most powerful pulsed neutron source with a large number of instruments. Together with other neutron scattering facilities in the world, it opens up huge opportunities for materials research. The neutron scattering can be used to probe the structure and dynamics of materials in a wide range of time and length scales. Compared to other characterization techniques, neutron scattering has its unique advantages, some of which are highly relevant for the study of battery materials. Firstly, neutrons interact directly with nuclei, and they, in general, do not interact with (paired) electrons. An obvious consequence of this is that neutrons can penetrate very deeply into the material, and neutron scattering is generally considered a bulk and non-destructive probe, a feature that will benefit greatly in-situ and/or in-operando studies. Secondly, the neutron scattering length or cross-section of a nucleus is determined by its atomic number and isotope (see Table 6). Its value in the periodic table seems to be quite random compared to the obvious trend with the cross-section of X-ray scattering: the latter simply scales with the atomic number or electron density. As a result, some light elements such as H, Li, O, and N have relatively high neutron scattering cross-sections, even higher than some heavy metals. This allows us to directly determine the coordinates of these light elements in the crystalline structure, and also allows us to obtain images of light elements from a background of heavier elements (contrary to the X-ray imaging). In addition, the neutron scattering length can be quite different between neighboring elements and different isotopes of the same element. This makes it possible to differentiate neighboring transition metals, study the effect of doping and explore isotope labeling. Thirdly, neutrons don't only have a wavelength comparable to interatomic distance, but their energy and momentum is also comparable to the fundamental excitations of vibration and diffusion. Therefore, compared to optical probes that use photons, the neutron is an ideal particle to study phonons and transport properties. Table 7 provides a list of neutron scattering techniques and a brief description of each technique. More details on specific techniques or more general applications in batteries and fuel cells can be found in the literature, including previous reviews [104–106]. Examples will be discussed in the following paragraphs.

Atomic structure

Similar to X-ray diffraction, neutron diffraction (ND) measures the atomic structure of materials. The mechanism is essentially the same, except that here the probe particles are neutrons instead of photons. As mentioned previously, this entails several advantages; one of them is that neutron diffraction can locate light elements such as Li, O, N [108–110]. This is important since the behavior of the material can sometimes be dictated by the concentration/distribution of lithium or the deficiency of oxygen. Neutron diffraction can also differentiate neighboring transition metals. Transition metal substitution is a common approach to modify the properties of electrodes and electrolytes. The ability to measure the distribution and ordering of transition metal elements (local and long-range) is critical. For example, $LiNi_{0.5}Mn_{1.5}O_4$ has been used as a high-voltage cathode material for all-solid-state batteries [111]. It is believed that the distribution of Ni and Mn in the "disordered" *Fd*-3*m* phase is random until recent neutron diffraction experiments show that there is

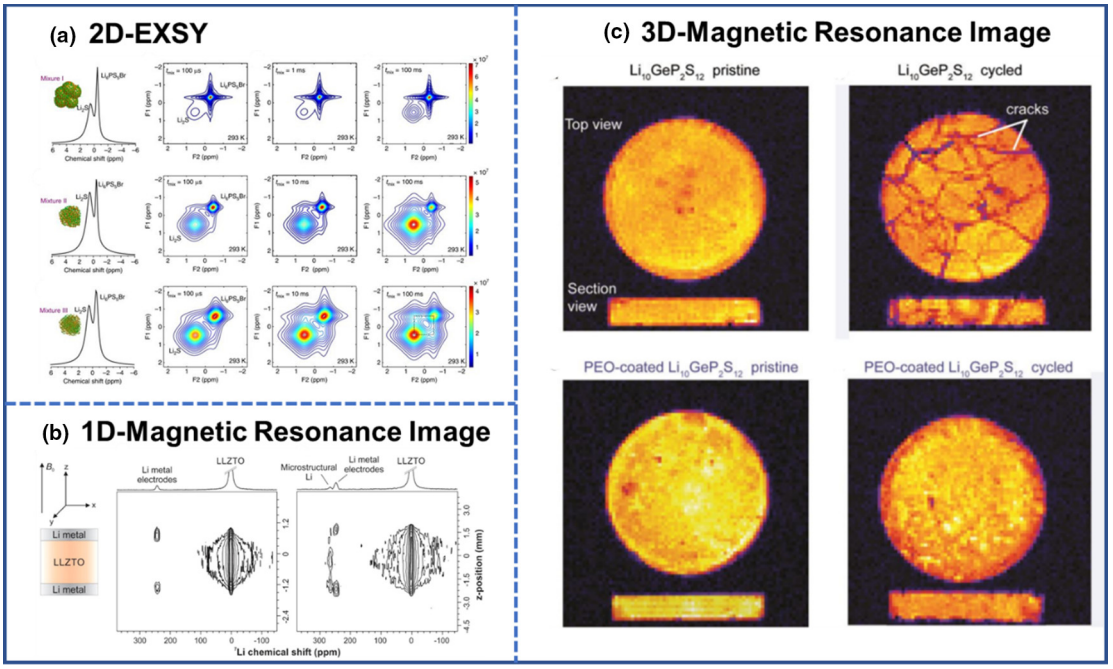

FIGURE 7

SS NMR techniques in the study of interfacial transport and morphology evolution. (a) 2D-Exchange spectroscopy. Copyright 2015, Nature Publishing House [73]. (b) One-dimensional magnetic resonance image, Copyright 2019, American Chemical Society [8] and (c) three-dimensional magnetic resonance image. Copyright 2018, American Chemical Society [74].

TABLE 6

Thermal neutron (E = 25.30 meV) scattering lengths and cross-sections for common elements in battery materials [107]·

Element/ isotope	Coherent scattering length (fm)	Total scattering cross-section (barn)	Absorption cross-section (barn)
H	−3.739	82.02	0.3326
D (^{2}H)	6.671	7.64	0.000519
Li	−1.90	1.37	70.5
^{6}Li (7.5%)	2.00–0.261i	0.97	940
^{7}Li (92.5%)	−2.22	1.4	0.0454
C	6.6460	5.551	0.0035
N	9.36	11.51	1.9
O	5.803	4.232	0.00019
P	5.13	3.312	0.172
S	2.847	1.026	0.53
Ti	−3.438	4.35	6.09
V	−0.3824	5.1	5.08
Mn	−3.73	2.15	13.3
Fe	9.45	11.62	2.56
Co	2.49	5.6	37.18
Ni	10.3	18.5	4.49
Zn	5.68	4.131	1.11

Note: In this table, what matters for diffraction (coherent scattering) is the scattering length; what matters for spectroscopy (under incoherent approximation) is the total scattering cross-section; what matters for imaging (attenuation) is the total cross-section (scattering plus absorption).

a significant local structural order in the Ni/Mn distribution, forming nanodomains of the ordered phase ($P4_332$) with disordered orientations [112,113]. This structural pattern has important implications on the behavior of the material, and the discovery was made possible by the fact that Mn has a negative neutron scattering length, so it can be easily distinguished from Ni (see Table 1). Such a hierarchical structure in solid electrolytes or electrode materials is not unusual and could be quite common. A recent study combining neutron powder diffraction (long-range order), pair distribution function (local order) and density functional theory (DFT) calculations revealed a complete structure image of lithium lanthanum titanate, which shows the coupling between the anti-phase TiO_6 rotation and the La-rich/poor super-lattice, as well as the twin boundaries between nanodomains with a size of about 5–10 nm [114]. Neutron

TABLE 7

Neutron scattering techniques and their applications.

Neutron scattering technique	What is measured and what can be learned
Neutron powder diffraction (NPD)	Crystal structure (space group, lattice constants, atomic coordinates)
Neutron total scattering (NTD)	Local structure (pair distribution function, nearest neighbor distance, and coordination)
Small-angle neutron scattering (SANS)	Nanostructure (size, morphology, and distribution)
Neutron Reflectometry (NR)	Surface and interface structure
Neutron depth profiling (NDP)	Distribution of an element as a function of depths into the solid
Neutron imaging (NI)	Contrast in neutron transmission/ attenuation
Inelastic neutron scattering (INS)	Vibrational dynamics (phonon dispersion and density of states)
Quasielastic neutron scattering (QENS)	Diffusive dynamics (diffusion coefficient and jump length)

diffraction has also been used to study amorphous electrolytes such as LiPON [115]. Despite its wide applications in solid-state thin-film batteries, the local structure in LiPON remained elusive and controversial. Specifically, it is believed that N in LiPON plays a critical role in determining the conductivity of Li, but the proposed local structure around N does not appear to be consistent with the material composition or theoretical prediction [115]. By combining the neutron pair distribution function (PDF) and DFT calculations, the structure of LiPON has finally been resolved (Fig. 8). Unlike the previously reported structure with double and triple bridging N, only the double bridging N and the apical N are found. It is also found that the presence of double-bridging N increases the conductivity of Li, while the apical N does not [115].

At longer length scales, the small-angle neutron scattering (SANS) measures the fluctuation of the scattering length density (SLD) in the order of 1 nm to 0.5 μm. The size and morphology of the nanoparticles or domains can be obtained by fitting the SANS data to various models. An important application of SANS in SSBs is to study copolymer electrolytes. The difference in H/D scattering length can be used to create contrast (that is, by partial deuteration). In a recent study, a solid-state battery using copolymer electrolyte was measured in operando with SANS [116]. The nanodomains were monitored with the battery running in severe working conditions and after more than 200 cycles. The electrolyte was found to be stable at 80 °C and 0.5 C, but began to show the inflation of the ionic pathways at 90 °C and 0.7 C [116]. In addition to the copolymers, SANS is also useful for characterizing composite solid electrolytes. For example, the SANS study of 3PEG nanocomposite polymer electrolytes filled with TiO_2 and Al_2O_3 revealed that filler particles, instead of having a uniform distribution in the polymer matrix, actually aggregate and form a network structure [117]. This supports the lithium conduction mechanism via the percolating network of the interface regions.

Interfacial investigation in solid-state battery

The neutron reflectometry and neutron depth profiling (NDP) are surface/interface probes, although their working mechanisms are quite different [104]. Neutron reflectometry is a type of neutron diffraction and measures the fluctuation of the neutron SLD as a function of depth. This method has been used to study the solid electrolyte interface (SEI) and lithium insertion/distribution. For example, it has been shown that silicon-based thin film is a promising anode material for all SSBs [118]. The incorporation of lithium in crystalline and amorphous silicon has been studied by neutron reflectometry [119,120]. These experiments took advantage of the negative scattering length of ^{7}Li, which makes it stand out from the background. NDP measures the distribution of certain elements based on depth. When neutrons react with ^{6}Li, tritium and alpha particles are generated. The charged particles lose energy while traveling to the surface, and the loss of energy depends on the distance they traveled. By measuring the final energy of the particles, one can, therefore, determine the initial location of the reaction, which leads to the distribution of the element of interest. This technique has been used to measure the distribution and cycle of Li in thin-film batteries [104].

On a much longer length scale beyond the atomic level or nanometers, the behavior of lithium-ion batteries can be tracked with neutron imaging [121,122]. Thanks to the large total cross-section of lithium (scattering plus absorption), it produces very good contrast with other elements in the system. The high neutron penetration allows operando studies to be performed to map the flow and distribution of lithium in real-time. This provides unique information that is not available in other characterization techniques and sheds light on issues related to battery design, electrochemical performance and cycle life. The spatial resolution that can be achieved with neutron imaging is of the order of 100 μm, and the new imaging beamline being constructed in SNS has an expected resolution of fewer than 15 μm.

Atomic-level dynamics

Unlike previous techniques, neutron spectroscopy measures the dynamics at the atomic level, such as vibration and diffusion. This is important to obtain a fundamental understanding of ion conduction processes. For ionic conductors, the diffusivity of conductive ions is a key property of the material. Although vibrational dynamics are on a much shorter time scale compared to diffusion, the way atoms vibrate can have important implications on how they diffuse, as revealed in recent studies that combine inelastic neutron scattering (INS) and computer modeling [123,124]. Specifically, it has been found that the average vibrational energy associated with conductive ions is closely related to the potential energy barrier for diffusion. Therefore, the average vibrational energy serves as a good indicator of ion mobility. One can imagine that vibrating ions naturally probe and examine their local potential energy profile, providing key information about their local environment. This correlation allows the prediction of the long-term behavior of ions from their short-term properties (Fig. 9).

Quasi-elastic neutron scattering (QENS) is the technology of choice for direct measurement of long-term scale behavior (i.e., diffusion). It measures the widening of the elastic line based on temperature, time, external field, etc. Such widening reflects the drift of an atom from its average position beyond vibration. With an energy resolution of the order of μeV, QENS can measure diffusive events on the nanosecond time scale. Combining with its spatial resolution determined by the Q range of the instrument, it is possible to solve the diffusion coefficients and the jump length of the events. QENS has traditionally been used to study hydrogenated materials primarily due to the large neutron scattering cross-section of hydrogen, but in recent years there have been many successful examples of using QENS to study the diffusion of lithium [125–128]. For example, the metastable superionic conductor $Li_7P_3S_{11}$ has received a lot of attention due to its high conductivity of Li. The rapid diffusion of lithium was measured directly with QENS, in which the self-diffusion constant, the mean residence time and the jump length were determined [126]. The jump length of 4.3 Å is consistent with the nearest neighboring Li–Li distance, suggesting that Li ions migrate between stable regions that percolate to form a Li-network in this metastable crystal. A summary of research performed with neutron scattering is given in Table 8. It should be noted that this brief summary is not intended to be a complete review of all related work done with neutron scattering. Instead,

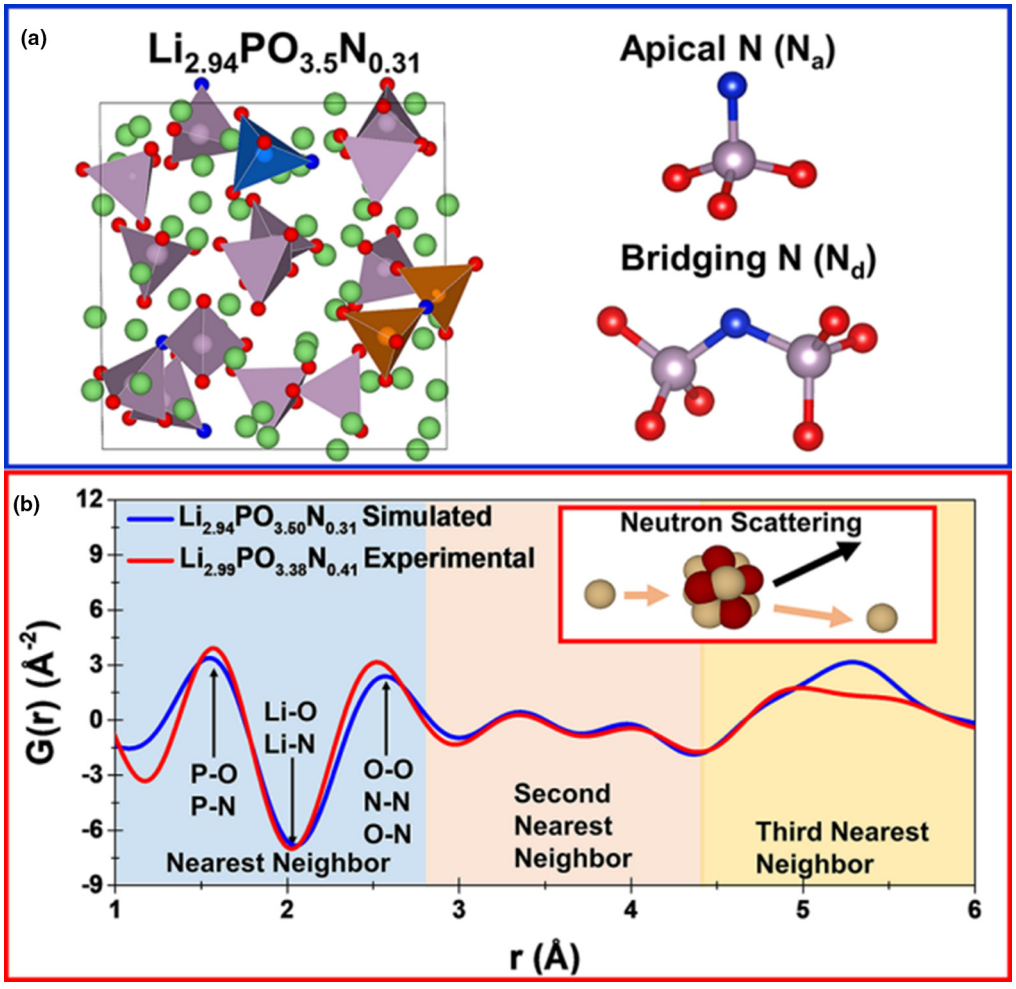

FIGURE 8

(a) A structural model of LiPON and (b) the neutron PDFs. Copyright 2018, American Chemical Society [115].

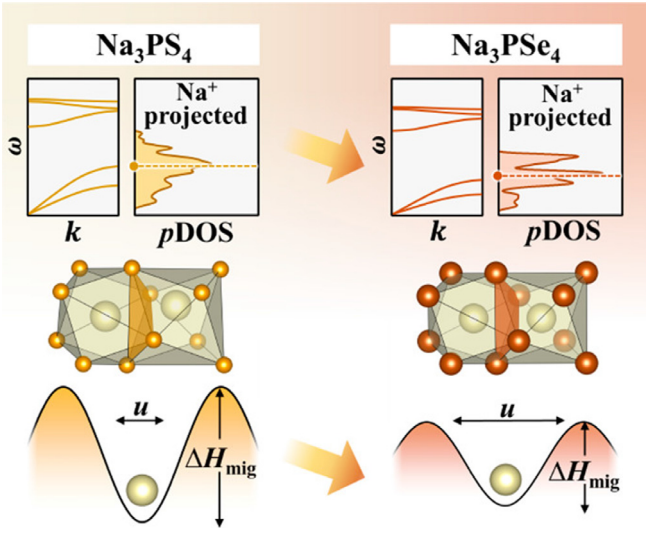

FIGURE 9

A schematic showing how the average vibrational energy is correlated with the energy barrier for diffusion and therefore the mobility of the conducting ions. Copyright 2018, American Chemical Society [123].

the goal here is to provide some examples of the application of each neutron scattering technique in all SSBs: what they measure and what we can learn from the data.

Summary and outlook

Solid-state batteries with high energy density and safety are considered a promising candidate for next-generation energy storage devices. However, its development still faces several challenges, including poor ionic conductivity, except for sulfide-based electrolytes, narrow electrochemical window and unstable solid electrode/chemical or electrochemical solid electrolyte interface. Further advances in these difficult issues depend on an in-depth understanding and insight into the mechanism of ionic transport and interfacial reaction, in particular, its evolution during the electrochemical cycle via advanced characterization techniques. In this review article, the characterization techniques that are significant and widely used in SSBs research are widely summarized. The advantages and uniqueness of each technique were illustrated by selected examples. The diverse information that includes crystal/local structure, chemical composition,

TABLE 8

Examples of solid-state battery research performed with neutron scattering.

	System	Method	Main issue addressed	Refs
Structure of SSEs	Li_3PO_4	ND	Site occupancy of Li and its elongation pathway	[109]
	$LiNi_{0.5}Mn_{1.5}O_4$	ND	Apparent incompatibility between local and global structure	[112,113]
	$Li_{3x}La_{(2/3-x)}TiO_3$	ND	Hierarchical local structure from atomic level to nanoscale	[114]
	$Li_7La_3Zr_2O_{12}$	ND	In situ observation of LLZO formation	[129]
	LiPON	ND	Bonding environment of N in amorphous LiPON	[115]
	Thio-LISICON	ND	Li diffusion pathway solved with maximum-entropy method	[108]
	3PEG–$LiClO_4$–TiO_2	SANS	Distribution of the filler particles (nano TiO_2 and Al_2O_3)	[117]
*Lithiation/delithiation and Li distribution (in-operando)	Li/LiPON/$LiCoO_2$	NDP	Li flow in each electrode	[104]
	Coin cell	NI	Lithiation and delithiation processes in thick sintered electrodes	[121]
	Coin cell	NI	3D distribution of Li in thin electrodes	[122]
	Commercial 18,650 cells	ND	Inhomogeneous reactions during charge and discharge processes	[110]
	DBC PS(d)-b-P (SPEG-co-STFSILi)	SANS	Cycling stability under operational conditions	[116]
	c-Si	NR	Evolution of Li depth profile within the Si anode and SEI	[119]
	a-Si	NR	Hysteretic behavior of lithiation and delithiation, as well as SEI formation and modification	[120]
Dynamics	$Na_3PS_{4-x}Se_x$	INS	Correlation between lattice dynamics and diffusion barrier	[123]
	Li_2S	QENS	Diffusion pathway between regular tetrahedral and interstitial octahedral sites and mean residence time	[125]
	$Li_7P_3S_{11}$	QENS	Self-diffusion constant, mean residence time, and jump length	[126]
	$xLi_2SO_4{\cdot}(1-x)LiPO_3$	QENS	Isotropic diffusion and composition dependence	[127]
	Li_xSi	QENS	Improved diffusion constant in defective Li_xSi	[128]
	$Li_5La_3Ta_2O_{12}$	QENS	Jump between tetrahedral (24 d) and octahedral (48 g and 96 h) sites	[130]

*Note: some of the in-operando studies are not on solid-state batteries but they demonstrate the unique capability of neutron scattering (thanks to its high penetration) to perform such measurements on solid-state batteries under working conditions.

bulk/interfacial heterogeneity and ionic movement provided by the synchrotron X-ray, SS NMR, and neutron scattering techniques are summarized and listed in Table 9. Some future development perspectives of each technique are presented below.

Due to the rapid development of SSBs and third-generation SR sources, various techniques, such as diffraction, spectroscopy, and imaging techniques, have been applied in the investigation of solid-state battery materials. It should be noted that the development of SSBs is still in the initial stage compared to the long history of the development of liquid-based batteries. Therefore, considering the future direction, the development of new SR techniques is of critical importance in the understanding and development of SSBs. Firstly, the application of in-situ SR techniques remains insufficient in the study of SSBs. For example, stability and purity are very important factors in the synthesis of solid state electrolytes. In-situ SXRD has been applied in solid state electrolyte research in terms of temperature and pressure to consider synthetic parameters. However, the evolution of non-crystalline structure materials cannot be reflected by SXRD, which needs more other in-situ X-ray characterizations to involve, such as XAS, XPS, PDF techniques, to provide chemical and electronics structure information of the materials. On the other hand, for the experimental setup, the development of the operando electrochemical cell configuration for SR techniques is significantly crucial, which should be able to obtain sufficient signal strength for characterization and operate the typical electrochemical behavior in the particular conditions at the synchrotron beamlines. In addition, time-resolved X-ray techniques with a rapid data acquisition time must be applied in the in-situ study of SSBs, which allows capturing the non-equilibrium state and the rapid transient process during electrochemical and chemical reactions. Secondly, the combination of several characterization techniques is important to obtain a complete picture and an exhaustive analysis in the investigation of SSBs. For example, the combination of X-ray microscopy and spectroscopy techniques can provide information on the morphological and chemical structure, which makes it possible to probe the heterogeneous and average characteristics of battery materials in SSBs. Finally, interfacial characterization is of great importance in SSBs, which need further development of SR techniques with improved spatial and temporal resolution. For example, state-of-the-art synchrotron-based X-ray imaging techniques can provide morphological and chemical information within the resolution of tens nanometers to millimeters, which remains a challenge to obtain images of interfacial evolution at the atomic length scale level (sub or few nm). Another example is that the synchrotron-based XPS allows to obtain the Li 1s spectrum, which is one of the few techniques that can directly probe the chemical structure of the Li element. The extremely superficial sensitivity of soft X-ray XPS techniques provides unique advantages to test the unstable chemical properties of Li metal and allows its application in the interface study between Li metal anode and SSEs, which will undoubtedly make a great contribution in the fundamental study of SSBs in the near future.

SS NMR is a powerful technique for studying the intrinsic properties of SSEs, such as site occupancy and ionic diffusion.

TABLE 9

A summary of diverse information provided by synchrotron X-ray techniques, SS NMR, and neutron scattering.

Techniques		Crystal Structure	Electronic structure	Interfacial reaction	Bulk/Interfacial heterogeneity	Ionic motion
Synchrotron X-ray	XRD	√		√		
	XPS		√	√	√	
	XAS		√	√	√	
	X-ray tomography			√	√	
SS NMR	MAS NMR	√	√	√		
	Dynamic NMR			√	√	√
	MRI			√	√	√
Neutron	ND	√		√		
	NR			√		
	NDP/SANS/NI				√	
	INS					√
	QENS					√

However, interfacial chemistry between the cathode/anode and solid-state electrolyte by using NMR techniques is rarely reported, which can be attributed to the small number of interfacial products and the poor NMR signal. Therefore, advanced NMR techniques with high resolution and sufficient signal intensity should be assessed and developed in the future. For example, in liquid-based batteries, the DNP (dynamic nuclear polarization) method has been used to study the components of interfacial products [131]. By transferring the nuclear spin hyperpolarization from ^{1}H to the studies nucleus, such as ^{6}Li,^{13}C and etc., the signal of the by-products of tracing can be greatly amplified and the experimental time is effectively shortened [131]. In contrast to the liquid-based batteries that contain the ^{1}H in the organic-electrolyte, lacking of ^{1}H in the solid-state batteries makes it difficult to perform the traditional DNP experiment. In this regard, the advanced endogenous DNP and relayed DNP are expected to play an important role in solid–solid interfacial analysis in future studies [132,133]. In addition, in the research of SSBs, most NMR experiments are based on post-mortem analysis, which would lose real information during the battery disassembly process. In-situ and/or in-operando NMR experiments are still insufficient in the study of SSBs, although it is crucial to investigate the mechanism of solid-state battery failure in working conditions. There are several challenges that must be addressed for in-situ and operando NMR as follows: (i) an in-situ SSBs configuration that with stable electrochemical cycles is imperative, especially with guaranteed pressure to maintain good solid–solid contact and undergo the volume change during cycling [134]; (ii) the limited temporal resolution that originated from the poor NMR signal; (iii) for MRI methods, unsatisfactory spatial resolution of only a few hundred micrometers. If these problems were effectively solved by the development of advanced NMR hardware and NMR pulse program, then in-situ configurations were combined with extensive NMR methods, such as MRI, PFG NMR and 2D EXSY, the spatial morphology and ionic movement are accessible in working conditions, which will provide significant help to solve essential scientific problems in SSBs.

As expected, the advantages of neutron scattering also come with some disadvantages, one of which is its low flux and brightness compared to synchronize X-rays, which means that it requires a relatively large amount of sample (from milligrams to grams, depending on the instrument and the source of neutrons used). To overcome the challenge so that more battery researchers can benefit from neutron scattering techniques, an important future direction is to develop brighter neutron sources, multimodal and higher resolution instruments, and advanced data analysis that integrates neutron scattering, simulation, and machine learning. Promising developments have been made. For example, it is expected that the second target station (STS) proposed in SNS, with a designed brightness 20 times greater than the first target station, will further expands the applications of neutron scattering in the investigation of batteries. High-performance computing with supercomputers is also being used to extract information and knowledge from neutron scattering data.

Compared to commercialized liquid batteries, SSBs are still in the initial stage of development and optimization. At present, the ionic conductivity of the optimized SSEs could satisfy the application of the SSBs [4]. Consequently, the main concern of SSBs research has gradually changed from improving the ionic conductivity of SSEs to addressing interface problems. As mentioned in previous reviews, the reaction and interfacial evolution during cycling are complex and elusive, which involves chemical, physical and mechanical issues [4]. For a comprehensive understanding of the relationship between structure and cycle performance, combinations of these advanced techniques are of great importance. For example, by combining XPS, NDP and the dynamic NMR method, the chemistry and ionic movement of the interface could be revealed. In addition, with the development of powerful computer techniques, the stable interface that facilitates ionic transport and improved SSBs stability could be predicted and new electrolytes could be selected using advanced theoretical calculations, etc. The combination and comparative analysis of theoretical calculations and experimental data will shed light on the rapid developments of the SSBs.

Acknowledgements

Y. Yang and his team would like acknowledge the long-term support of their research from National Natural Science Foundation of China (Grant number: (21935009, 21761132030). X. Sun and his team would like acknowledge Natural Sciences and Engineering Research Council of Canada (NSERC), Canada Research Chair Program (CRC), Canada Foundation for Innovation (CFI), Ontario Research Fund (ORF), and Western University. Xia Li thanks to the support of Mitacs Elevate Postdoctoral Fellowship. Y.Q. Cheng's work at the Spallation Neutron Source was supported by the Scientific User Facilities Division, Office of Basic Energy Sciences, U.S. Department of Energy, under Contract No. DE-AC0500OR22725 with UT Battelle, LLC.

References

[1] P. Albertus et al., Nat. Energy 3 (1) (2018) 16.
[2] J. Liu et al., Nat. Energy (2019).
[3] X.B. Cheng et al., Chem. Rev. 117 (15) (2017) 10403.
[4] Y. Shen et al., Joule 2 (9) (2018) 1674.
[5] B. Zheng et al., ACS Appl. Mater. Interfaces 10 (30) (2018) 25473.
[6] Y. Ruan et al., J. Mater. Chem. A 7 (24) (2019) 14565.
[7] J. Dai et al., Adv. Mater. 30 (48) (2018) 1802068.
[8] L.E. Marbella et al., Chem. Mater. 31 (8) (2019) 2762.
[9] X. Li et al., ACS Energy Lett. 4 (10) (2019) 2480.
[10] F. Lin et al., Chem. Rev. 117 (21) (2017) 13123.
[11] P. Oliver et al., Chem. Mater. 29 (1) (2016) 213.
[12] W. Li et al., Small Methods 2 (8) (2018) 1700341.
[13] W. Huang et al., Adv. Energy Mater. 7 (21) (2017) 1700460.
[14] C.H. Wu et al., PCCP 17 (45) (2015) 30229.
[15] L. Buannic et al., Chem. Mater. 29 (4) (2017) 1769.
[16] S.-M. Bak et al., NPG Asia Mater. 10 (7) (2018) 563.
[17] E. Hu et al., Acc. Chem. Res. 51 (2) (2018) 290.
[18] D.H. Bilderback et al., J. Phy. B 38 (9) (2005) S773.
[19] A. Sakdinawat, D. Attwood, Nat. Photon. 4 (12) (2010) 840.
[20] D. Safanama et al., J. Mater. Chem. A 4 (20) (2016) 7718.
[21] C. Wang et al., Small Methods (2019) 1900261.
[22] Y. Liu et al., ACS Appl. Mater. Interfaces 10 (37) (2018) 31240.
[23] N. Seitzman et al., J. Electrochem. Soc. 165 (16) (2018) A3732.
[24] B. Wu et al., J. Mater. Chem. A 4 (40) (2016) 15266.
[25] A. Manthiram et al., Nat. Rev. Mater. 2 (3) (2017) 16103.
[26] J.C. Bachman et al., Chem. Rev. 116 (1) (2016) 140.
[27] R. Chen et al., Mater. Horizons (2016).
[28] I. Robinson, R. Harder, Nat. Mater. 8 (4) (2009) 291.
[29] I.K. Robinson, D.J. Tweet, Rep. Prog. Phys. 55 (5) (1992) 599.
[30] G. Renaud et al., Surf. Sci. Rep. 64 (8) (2009) 255.
[31] Y. Sun et al., J. Power Sources 324 (2016) 798.
[32] L. Cheng et al., ACS Appl. Mater. Interfaces 7 (3) (2015) 2073.
[33] H. Wang et al., J. Power Sources 401 (2018) 111.
[34] C. Dietrich et al., Inorg. Chem. 56 (11) (2017) 6681.
[35] L. Cheng et al., ACS Appl. Energy Mater. 1 (12) (2018) 7244.
[36] M. Duchardt et al., Angew. Chem. Int. Ed. Engl. 57 (5) (2018) 1351.
[37] R. Kun et al., ACS Appl. Mater. Interfaces 10 (43) (2018) 37188.
[38] A.A. Hubaud et al., J. Alloys Compd. 644 (2015) 804.
[39] E. Kazyak et al., Chem. Mater. 29 (8) (2017) 3785.
[40] Y. Meesala et al., J. Phys. Chem. C 122 (26) (2018) 14383.
[41] J. Rao et al., J. Phys. Chem. C 122 (26) (2018) 14546.
[42] H. Stöffler et al., J. Phys. Chem. C 122 (28) (2018) 15954.
[43] K. Xu, Chem. Rev. 114 (23) (2014) 11503.
[44] M.F. Groh et al., Chem. Mater. 30 (17) (2018) 5886.
[45] S. Shiraki et al., ACS Appl. Mater. Interfaces (2018).
[46] T. Hakari et al., Chem. Mater. 29 (11) (2017) 4768.
[47] K. Chen et al., Solid State Ionics 327 (2018) 150.
[48] C. Dietrich et al., PCCP 20 (30) (2018) 20088.
[49] Y. Fujii et al., J. Electrochem. Soc. 165 (13) (2018) A2948.
[50] G. Vardar et al., Chem. Mater. 30 (18) (2018) 6259.
[51] M. Sing et al., Phys. Rev. Lett. 102 (17) (2009) 176805.
[52] X. Liu et al., Adv. Mater. 26 (46) (2014) 7710.
[53] J. Zhong et al., Adv. Mater. 26 (46) (2014) 7786.
[54] A. Bianconi, Appl. Surf. Sci. 6 (3–4) (1980) 392.
[55] D.E. Sayers et al., Phys. Rev. Lett. 27 (18) (1971) 1204.
[56] Z. Gong, Y. Yang, J. Energy Chem. 27 (6) (2018) 1566.
[57] F. Shen et al., ACS Energy Lett. 3 (4) (2018) 1056.
[58] T. Li et al., ACS Appl. Mater. Interfaces 10 (20) (2018) 16927.
[59] F. Sun et al., J. Mater. Chem. A 6 (45) (2018) 22489.
[60] M.M. Besli et al., Chem. Mater. 31 (2) (2018) 491.
[61] Y.-X. Xiang et al., Solid State Ionics 318 (2018) 19.
[62] P. Heitjans, J. Kärger, Diffusion in Condensed Matter: Methods, Materials, Models, Springer Science & Business Media, 2006.
[63] M. Wilkening, P. Heitjans, ChemPhysChem 13 (1) (2012) 53.
[64] D. Wang et al., J. Mater. Chem. A 2 (47) (2014) 20271.
[65] Y. Deng et al., Chem. Mater. 30 (8) (2018) 2618.
[66] D. Rettenwander et al., Chem. Mater. 27 (8) (2015) 3135.
[67] A. Kuhn et al., Energy Environ. Sci. 6 (12) (2013) 35.
[68] C. Yu et al., J. Mater. Chem. A 5 (40) (2017) 21178.
[69] C. Yu et al., ACS Appl. Mater. Interfaces 10 (39) (2018) 33296.
[70] B. Stanje et al., Ann. Phys. 529 (2017) 12.
[71] S. Ganapathy et al., ACS Energy Lett. (2019) 1092.
[72] D. Wang et al., Chem. Mater. 27 (19) (2015) 6650.
[73] Y. Chuang et al., Nat. Comm. 8 (1) (2017) 1086.
[74] P.H. Chien et al., J. Phys. Chem. Lett. 9 (8) (2018) 1990.
[75] A. Marchetti et al., Adv. Mater. 29 (14) (2017) 1605895.
[76] J. Keeler, Understanding NMR Spectroscopy, John Wiley & Sons, 2011.
[77] M.H. Levitt, Spin Dynamics: Basics of Nuclear Magnetic Resonance, John Wiley & Sons, 2001.
[78] L. van Wullen et al., PCCP 9 (25) (2007) 3298.
[79] A.A. Hubaud et al., J. Mater. Chem. A 1 (31) (2013) 8813.
[80] K. Arbi et al., PCCP 16 (34) (2014) 18397.
[81] C. Vinod Chandran et al., J. Phys. Chem. C 120 (16) (2016) 8436.
[82] K. Arbi et al., ChemInform 33 (2010) 24.
[83] B. Key et al., Chem. Mater. 24 (2) (2012) 287.
[84] R. Kahlaoui et al., Inorg. Chem. 56 (3) (2017) 1216.
[85] J. Emery et al., J. Phys. Chem. C 120 (46) (2016) 26173.
[86] X. Feng et al., Adv. Funct. Mater. 29 (2019) 9.
[87] S. Harm et al., Chem. Mater. 31 (4) (2019) 1280.
[88] Y. Deng et al., J. Am. Chem. Soc. 137 (28) (2015) 9136.
[89] Y. Chuang et al., J. Mater. Chem. A (2016).
[90] X. Liang et al., Chem. Mater. 27 (16) (2015) 5503.
[91] D. Yue et al., Chem. Mater. (2018).
[92] J. Zheng, Y.-Y. Hu, ACS Appl. Mater. Interfaces 10 (4) (2018) 4113.
[93] A.A. Savina et al., Chem. Mater. 29 (20) (2017) 8901.
[94] R. Bhattacharyya et al., Nat. Mater. 9 (2010) 504.
[95] F. Aguesse et al., ACS Appl. Mater. Interfaces 9 (4) (2017) 3808.
[96] R. Murugan et al., Angew. Chem. Int. Ed. Engl. 46 (41) (2007) 7778.
[97] H. Buschmann et al., PCCP 13 (43) (2011) 19378.
[98] D. Rettenwander et al., Chem. Mater. 26 (8) (2014) 2617.
[99] D. Wang et al., Solid State Ionics 283 (2015) 109.
[100] Y. Ting et al., ACS Appl. Mater. Interfaces (2017).
[101] J. Zheng et al., Angew. Chem. Int. Ed. Engl. 55 (40) (2016) 12538.
[102] E.M. Lauren et al., Chem. Mater. (2019).
[103] T.E. Mason et al., Physica B 385–386 (2006) 955.
[104] H. Wang et al., In situ neutron techniques for studying lithium ion batteries, in: Polymers for Energy Storage and Delivery: Polyelectrolytes for Batteries and Fuel Cells, American Chemical Society, 2012, p. 91.
[105] Y. Ren, X. Zuo, Small Methods 2 (8) (2018) 1800064.
[106] A.M. Balagurov et al., Russ. Chem. Rev. 83 (12) (2014) 1120.
[107] V.F. Sears, Neutron News 3 (3) (1992) 26.
[108] N. Minafra et al., Chem. Mater. 31 (10) (2019) 3794.
[109] E. Kartini et al., Physica B (2017).
[110] S. Taminato et al., Sci. Rep. 6 (2016) 28843.
[111] G. Oh et al., Chem. Mater. 28 (8) (2016) 2634.
[112] J. Liu et al., Chem. Mater. 28 (19) (2016) 6817.
[113] Y. Chen et al., Adv. Energy Mater. 7 (2017) 4.
[114] Y.Q. Cheng et al., J. Mater. Chem. A 2 (7) (2014) 2418.
[115] V. Lacivita et al., J. Am. Chem. Soc. 140 (35) (2018) 11029.
[116] G.E. Mohl et al., ACS Energy Lett. 3 (1) (2018) 1.
[117] C. Karlsson et al., Macromolecules 38 (15) (2005) 6666.
[118] J. Sakabe et al., Commun. Chem. 1 (1) (2018) 24.
[119] B.K. Seidlhofer et al., ACS Nano 10 (8) (2016) 7458.
[120] B. Jerliu et al., PCCP 20 (36) (2018) 23480.
[121] Z. Nie et al., J. Power Sources 419 (2019) 127.
[122] Y. Zhang et al., J. Power Sources 376 (2018) 125.
[123] T. Krauskopf et al., J. Am. Chem. Soc. 140 (43) (2018) 14464.

[124] Y. Cheng et al., J. Mater. Chem. A 5 (30) (2017) 15507.
[125] F. Altorfer et al., J. Phys.: Condens. Matter 6 (46) (1994) 9937.
[126] K. Mori et al., Phys. Rev. Appl 4 (2015) 5.
[127] T. Heitmann et al., Solid State Ionics 334 (2019) 95.
[128] R.L. Sacci et al., J. Phys. Chem. C 121 (21) (2017) 11083.
[129] R.P. Rao et al., Chem. Mater. 27 (8) (2015) 2903.
[130] M.J. Klenk et al., Solid State Ionics 312 (2017) 1.
[131] J. Yanting et al., J. Am. Chem. Soc. (2017).
[132] S. Björgvinsdóttir et al., J. Am. Chem. Soc. 140 (25) (2018) 7946.
[133] T. Wolf et al., J. Am. Chem. Soc. 141 (1) (2019) 451.
[134] J. Sakamoto, Nat. Energy 4 (10) (2019) 827.